Geochemistry, Geophysics, Geosystems

RESEARCH ARTICLE
10.1029/2018GC007894

Special Section:
Magnetism in the Geosciences - Advances and Perspectives

Particle Size Specific Magnetic Properties Across the Norwegian-Greenland Seas: Insights Into the Influence of Sediment Source and Texture on Bulk Magnetic Records

Robert G. Hatfield[1], Benjamin H. Wheeler[1,2], Brendan T. Reilly[1], Joseph S. Stoner[1], and Bernard A. Housen[3]

[1]College of Earth, Ocean, and Atmospheric Sciences, Oregon State University, Corvallis, OR, USA, [2]School of Earth and Sustainability, Northern Arizona University, Flagstaff, AZ, USA, [3]Geology Department, Western Washington University, Bellingham, WA, USA

Key Points:
- The magnetic properties of five particle size fractions reveal the controls on the bulk magnetic signal across the Norwegian-Greenland Seas
- Ferrimagnetic fragments preferentially reside in the silt-size fractions and silt is a dominant control on bulk magnetic susceptibility
- Hysteresis and low-temperature magnetic susceptibility behavior permits the discrimination and fingerprinting of three distinct sediment sources

Correspondence to:
R. G. Hatfield,
rhatfield@ceoas.oregonstate.edu

Citation:
Hatfield, R. G., Wheeler, B. H., Reilly, B. T., Stoner, J. S., & Housen, B. A. (2019). Particle size specific magnetic properties across the Norwegian-Greenland seas: Insights into the influence of sediment source and texture on bulk magnetic records. *Geochemistry, Geophysics, Geosystems*, *20*, 1004–1025. https://doi.org/10.1029/2018GC007894

Received 23 AUG 2018
Accepted 19 JAN 2019
Accepted article online 24 JAN 2019
Published online 15 FEB 2019

Abstract We make fundamental observations of the particle size variability of magnetic properties from 71 core tops that span the southern Greenland and Norwegian Seas. These data provide the first detailed regional characterization of how bulk magnetic properties vary with sediment texture, sediment source, and sediment transport. Magnetic susceptibility (MS) and hysteresis parameters were measured on the bulk sediment and the five constituent sediment particle size fractions (clay, fine silt, medium silt, coarse silt, and sand). The median MS value of the medium silt size fraction is ~3–5 times higher than that of the sand and clay size fractions and results in a strong sensitivity of bulk MS to sediment texture. Hysteresis properties of the clay size fraction are relatively homogeneous and contrast that silt and sand size fractions which show regional differences across the study area. These coarser fractions are more transport limited and using medium silt hysteresis measurements and low temperature MS behavior we establish three endmembers that effectively explain the variability observed across the region. We model the response of bulk magnetic properties to changes in sediment texture and suggest that variations in sediment source are required to explain the bulk magnetic property variability observed in cores across the southern Greenland and Norwegian Seas. These findings imply that sediment source has a greater influence on driving bulk magnetic property variability across this region than has previously been assumed.

Plain Language Summary Sediments from the bottom of the ocean can tell us about past environmental conditions (climate, ocean circulation, ice sheet growth, and retreat) that we cannot obtain by other means. Naturally occurring iron-bearing minerals in the sediment are strongly sensitive to changing environmental conditions and can be rapidly and nondestructively characterized by using a suite of magnetic property measurements. To better understand these records we split bulk sediments recovered from 71 locations across the Norwegian and Greenland Seas into five different grain size ranges and made the same magnetic measurements on each size fraction and the bulk sediment. The silt-size fractions contain several times the amount of magnetic material than the clay- or sand-size fractions resulting in a strong dependence of bulk properties on the presence of clay, silt, and sand. Sediment source also strongly influences silt and bulk magnetic properties and by sampling widely across the study region we present new evidence for source-driven variability that was not previously known. These findings suggest that we need to consider how changes in sediment source and sediment grain size might affect interpretations of bulk sediment magnetic properties. These new insights can provide detailed new information about Earth's past.

1. Introduction

Bulk (whole sample) magnetic properties of marine sediment cores recovered from the northern North Atlantic (NNA) have repeatedly shown sensitivity to millennial and orbital scale variations in environmental conditions (Ballini et al., 2006; Hatfield et al., 2016; Kissel et al., 1999, 2008, 2009; Robinson, 1986; Robinson et al., 1995; Snowball & Moros, 2003; Stoner & Andrews, 1999). Magnetic susceptibility (MS) is one of the most frequently acquired physical property measurements on bulk sediment cores and provides a first-order approximation of the concentration of ferrimagnetic minerals (e.g., magnetite, titanomagnetite, maghemite) that are ubiquitous in the lithogenic fraction of North Atlantic

marine sediments (Robinson, 1986; Stoner & Andrews, 1999) and their terrestrial sources (Hatfield et al., 2013, 2017; Watkins & Maher, 2003). Additional magnetic parameters and ratios (e.g., hysteresis properties, the S-ratio, karm/k, and the temperature dependence of MS) are sensitive to magnetic grain size and magnetic mineralogy and can reflect different sources of the magnetic fraction (Bloemendal et al., 1992; Hatfield et al., 2013, 2017; Stoner et al., 1995, 1996; Watkins & Maher, 2003). Together this suite of magnetic measurements has been used to trace the delivery of ice rafted debris (IRD) to the open ocean (Grousset et al., 1993; Robinson, 1986; Stoner & Andrews, 1999), reconstruct the growth and demise of continental size ice-sheets (e.g., Hatfield et al., 2016; Stoner et al., 1995), and track variations in the strength and migration of deep ocean currents (Ballini et al., 2006; Kissel et al., 1999; Moros et al., 1997; Rasmussen et al., 1996).

The advantage of using bulk magnetic measurements as paleo-proxies are their relative ease, speed, and nondestructive nature of measurement coupled with their strong sensitivity to environmental change. However, because magnetic properties are sensitive to a range of different processes and because bulk measurements are an average all the different components present in the bulk sediment, it can often be difficult to determine the specific drivers of bulk magnetic variation. For example, magnetic properties in the NNA vary strongly between source regions (Hatfield et al., 2013; Watkins & Maher, 2003) and can be strongly dependent on sediment grain size (Hatfield et al., 2016, 2017; Lascu et al., 2015) meaning that sediment sourcing and sediment texture variations can both influence bulk magnetic properties. Particle size specific magnetic measurements provide a method to separate these two processes and an assessment of their influence in driving bulk magnetic changes (Hatfield, 2014). However, detailed particle size specific magnetic observations of NNA sediments are relatively rare and have thus far been limited to characterization of terrestrial sediments from Greenland and Iceland (Hatfield et al., 2013, 2017), analysis of a marine sediment core south of Greenland (Hatfield et al., 2016), and a comparison of several spatially disparate core tops (Lascu et al., 2015). These studies have repeatedly highlighted the strong particle size dependence of magnetic properties and the importance of sediment provenance in driving bulk magnetic variability. However, without a dedicated assessment it is unclear whether these findings are representative of the wider NNA picture.

Here we make bulk and particle size specific magnetic measurements on 71 core tops that span the coastal margins of east Greenland, western Norway, Jan Mayen, and Iceland across the southern Norwegian and Greenland Seas (Figure 1). This vast array represents the first large-scale characterization of particle size specific magnetic properties in the NNA and permits examination of not only sediment texture, but also because of the spatial scale, the potential for sediment source variability. These cores encompass a region frequently referred to as the Nordic Basaltic Province (NBP) which is often considered an important source of the ferrimagnetic fraction to the wider NNA basin (Ballini et al., 2006; Kissel et al., 1999, 2009; Snowball & Moros, 2003). Terrestrial exposures across the NBP are dominated by Paleogene and Neogene basalt (Kissel et al., 1999; Laj et al., 2002) and it is generally considered that NBP sediments are dominated by free (i.e., not included in other minerals or aggregates), low titanium content, magnetite (e.g., Ballini et al., 2006; Kissel et al., 1999). Under this assumption the downcore variability in MS and magnetic grain size in NBP and NNA cores has frequently been explained by changes in the strength of bottom currents and their capacity to entrain and transport the ferrimagnetic fraction (Ballini et al., 2006; Kissel et al., 1999; Moros et al., 1997; Snowball & Moros, 2003). To investigate the particle size specific magnetic variability across this region the core top sediments were first separated into five particle size fractions (clay, three silt-size fractions, and sand). Magnetic measurements were then made on the five sediment fractions and the bulk sediment to characterize magnetic concentration, magnetic mineralogy, and magnetic grain size variability. These observations help determine the sensitivity of bulk magnetic properties to sediment texture and sediment source variations and provide new insights for the interpretation of bulk magnetic property records across this region and the wider NNA.

2. Materials and Setting

The Norwegian and Greenland seas are an important region in the formation of North Atlantic Deep Water and, accordingly, the global oceanic redistribution of heat between hemispheres. Warmer salty surface waters that are transported north in the Gulf Stream, cool, and sink to depths >3,000 m in the Nordic Seas, before returning in bottom water currents that hug the submarine topography. These bottom currents are capable of mobilizing and entraining the sediments they encounter before climbing and overflowing the

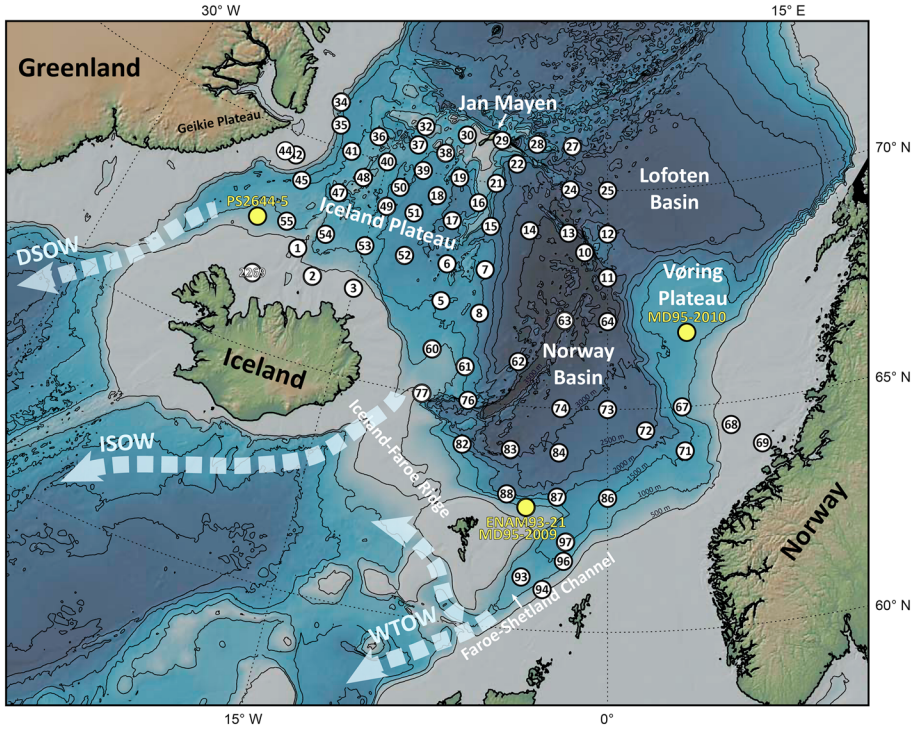

Figure 1. Location of the 70 Edisto cores and core MD99-2269 (white and numbered) and cores ENAM93-21, MD95-2009, MD95-2010, and PS2644-5 that are discussed in the text (yellow). Dashed arrows show the path of major overflow waters from the Nordic seas to the wider North Atlantic. DSOW = Denmark Strait Overflow Water; ISOW = Iceland Scotland Overflow Water; WTOW = Wyville Thompson Overflow Water.

shallow sill (400–650 m water depth) that separates the Greenland and Norwegian seas from the wider North Atlantic Ocean. Overflows occur through several gateways including the Denmark Strait as Denmark Strait overflow water, between Iceland and the Faroe Islands as Iceland-Scotland overflow water, and through the Faroe-Shetland Channel as Wyville Thompson ridge overflow water (Figure 1). Lithogenic sediments across this region have several potential sources, including the terrestrial glaciated margins of Greenland, Norway, Iceland and Jan Mayen, and submarine exposures along the mid-ocean ridge.

Seventy of the surface samples are from piston cores retrieved during the 1963 expedition of the RV Edisto (ED-1963-01 to ED-1963-94; hereinafter referred to as cores 01 to 94). Following recovery the Edisto cores were stored at room temperature at the University of Washington before being transferred to Oregon State University in 1989. The other core top sample is from calypso core, MD99-2269, that was recovered in 1999 during the IMAGES V cruise aboard the Marion Dufrense (Turon et al., 1999) and curated at Woods Hole Oceanographic Institution and Oregon State University at 4 °C. Together these 71 cores form an array (hereinafter called the Edisto Array) bounded to the south by the Iceland-Faroe Ridge and the Faroe-Shetland Channel, to the north by the Jan Mayen fracture zone and the Vøring Spur, and to the east and west by the continental margins of Norway and Iceland and Greenland (Figure 1). The cores were recovered from water depths between 181 and 3,658 m (Figure 1) though the western half of the array across the Iceland Plateau is shallower (<~2,100 m) than the eastern half which sinks to depths in excess of 3,500 m in the Norway Basin. The recovered sediments encompass a range of colors, textures, lithologies, and biogenic components (e.g., Bjørklund et al., 1998) that reflect the heterogeneous mixture of sources and depositional regimes across the region. Due to complex deposition, transport, and resuspension processes that likely include rapid accumulation and strong winnowing it is unlikely that all the core top sediments represent the same time horizon. However, as our aim is not to investigate temporal change, but characterize the sediment variability across the region, any differences in the age of the surface sediments should not significantly affect this investigation.

3. Methods

Bulk sediment was sampled from the top 2 cm of each of the 71 cores and split in two subsamples; the first was used for measurement of bulk magnetic properties, and the second was separated into five particle size fractions. Samples for fractionation were agitated with 100 ml of a 2% sodium hexametaphosphate solution to disaggregate the bulk sediment and then passed through 63 and 32 μm sieves to generate sand (>63 μm) and coarse silt (32–63 μm) sediment fractions. The residual <32 μm fraction was fractionated in settling columns according to Stoke's law to generate three sediment fractions; medium silt (10–32 μm), fine silt (2–10 μm), and clay (<2 μm). Each column separation was repeated twice (for a total of three runs at each step) to reduce fine fraction contamination of the coarser separate. Samples were air dried at 40 °C and weighed to calculate the mass of each fraction and percent abundance in the bulk sediment.

For the 71 bulk and 355 particle size fractions ~100–200 mg of sediment was immobilized in gelatin caps for measurement of room temperature MS and hysteresis properties. MS was measured three times and averaged using a Kappabridge KLY-2 at a frequency of 920 Hz in a 300 A/m field. Saturation magnetization (M_s), saturation remanence (M_{rs}), and coercivity (H_c) data were derived from the major hysteresis loop measured to a saturating field of 1,000 mT and corrected for paramagnetic contributions using the high field slope above 800 mT. The coercivity of remanence (H_{cr}) was determined by demagnetization of the 1,000 mT IRM in 2.5 mT steps. High field susceptibility (χ_{HF}) is sensitive to diamagnetic and paramagnetic contributions and was calculated using the slope correction of the hysteresis data following Brachfeld (2006). First-order reversal curves (FORCs) were measured on six medium silt fractions and are composed of 247 individual FORCs measured with averaging times of 150–500 m/s and a peak field of 500 mT. FORCs were smoothed using VARIFORC (Egli, 2013) in the FORCinel 3.0 processing software of Harrison and Feinberg (2008). All hysteresis and FORC measurements were made on a Princeton Measurements Corporation Micromag model 3900 vibrating sample magnetometer. To separate the influence of magnetic mineralogy from magnetic grain size variations that can influence hysteresis properties in similar ways (e.g., Roberts et al., 2018) the low temperature dependence of MS (LTMS) was measured on 21 medium silt fractions. Samples (~300–500 mg weight) were cooled in liquid nitrogen to ~80 K and MS was measured every 1–2 K during warming to ~273 K on a Kappabridge KLY-2 at a frequency of 920 Hz in a 300 A/m field. MS outliers were removed and the profiles were smoothed prior to normalization using the MS value measured at 273 K following Hatfield et al. (2017). All magnetic measurements were made at the Pacific Northwest Paleomagnetic Laboratory at Western Washington University. Spatial interpolations of the magnetic and particle size data were performed in QGIS using an inverse distance weighting algorithm provided by SAGA (System for Automated Geoscientific Analyses) that allowed for greater flexibility in settings (power = 10, weight = exponential, cell size = 0.1, search range = global) over the standard toolbox.

4. Results

4.1. Physical Particle Size Variability

As the sediments were not chemically treated to remove biogenic components bulk samples are dominantly composed of a mix of lithogenic fragments and biogenic carbonates and silicates. The abundance of biogenic materials varies between samples, but following fractionation of the bulk sediment the biogenic components generally reside in the >63 μm (sand size) fraction. As a result the sand fraction has the most variable abundance, ranging between 0.5% and 61% (median = 17%) of the bulk sediment (Figure 2). For 10 of the cores sand is the most abundant size fraction (Figure 2), and in 7 of those samples (excluding cores 1, 2, and 3 on the Iceland shelf), foraminiferal tests are the dominant component. However, for the majority of cores ($n = 61$) the fine silt (median abundance = 35%) and clay (median = 24%) fractions are the most abundant, followed by the medium silt (median = 13%) and coarse silt (median = 6%) fractions (Figure 2).

The proportion of clay shows little to no relationship with water depth across the Edisto Array (Figure 3a), although clay does appear to be slightly more abundant along the Greenland and Norwegian margins (Figure 2). The ubiquity of clay across all water depths likely reflects the high transport potential of the finest fraction that, once mobilized, can be relatively easily redistributed across the entire basin. Negative correlation of the proportion of medium ($r = -0.57$) and coarse ($r = -0.46$) silt fractions with water depth (Figure 3) suggests that noncohesive (>10 μm) silt fractions are more abundant in shallower water depths closer to continental margins. Lower abundances in deeper water (e.g., the Norway Basin) may reflect a more limited

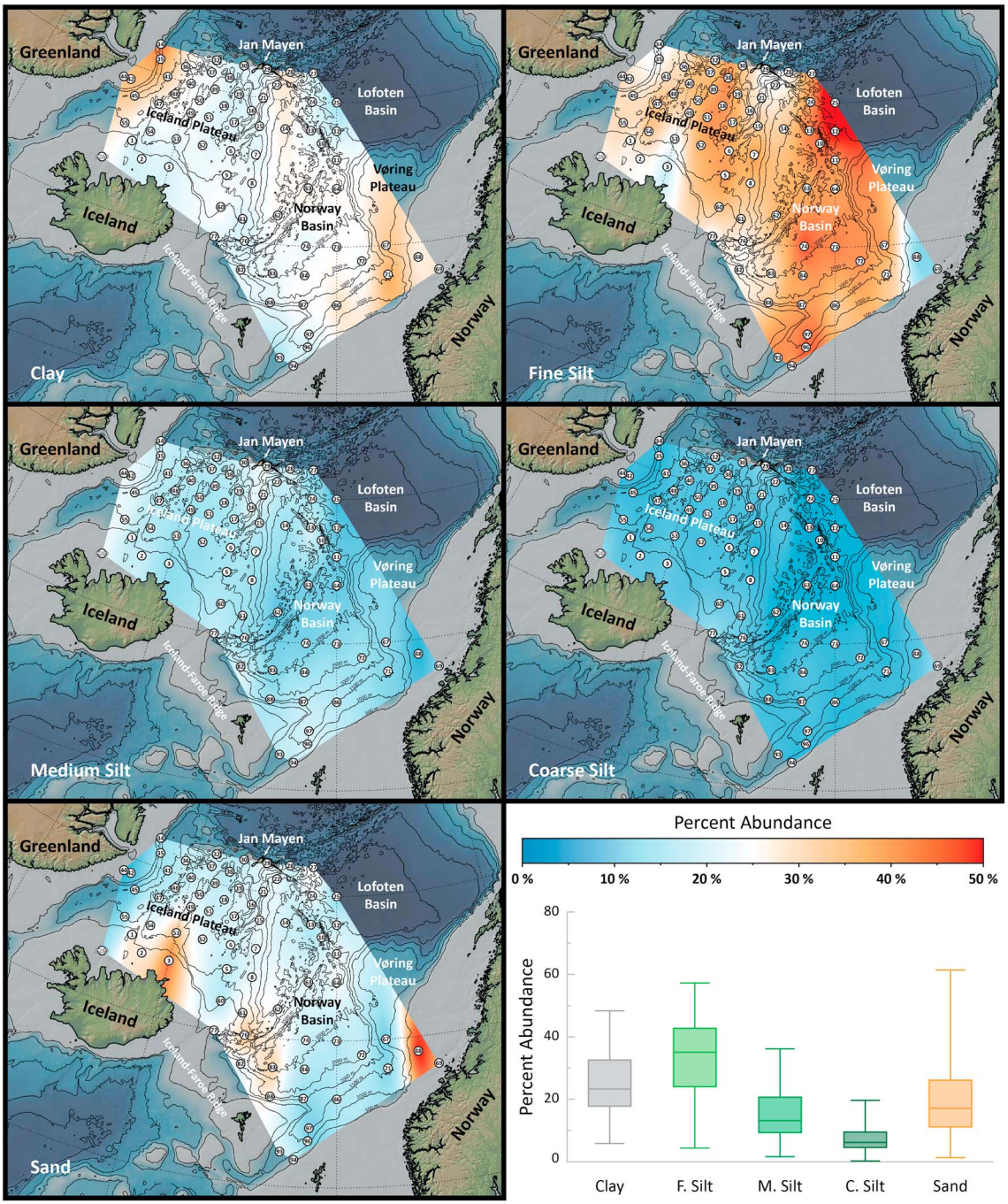

Figure 2. Percent abundance of clay (<3 μm), fine silt (3–10 μm), medium silt (10–32 μm), coarse silt (32–63 μm), and sand (>63 μm) in the 71 cores that constitute the Edisto Array. Also shown are the median (central bar), upper and lower quartiles (box), and maximum and minimum values (bars) for each size fraction (lower right). Fine silt is the most abundant fraction across the array followed by clay, medium silt, and fine silt. Sand is the most variable fraction across the array resulting from contributions of biogenic and lithogenic components (see text).

transport potential of these coarser sediment fractions relative to the finer, cohesive (<10 μm), fractions. The complete sand-size abundance data set shows no relationship with water depth (Figure 3e). However, if we separate the sands into two populations based on their MS values then the split with higher MS (interpreted to have a greater proportion of lithogenic fragments) is confined to water depths less than ~2,100 m, while the lower MS split (higher biogenic contributions) spans the full water depth range from ~300 to 3,700 m (Figure 3e). The higher MS split ($r = -0.58$; Figure 3f) is then consistent with the source-proximal

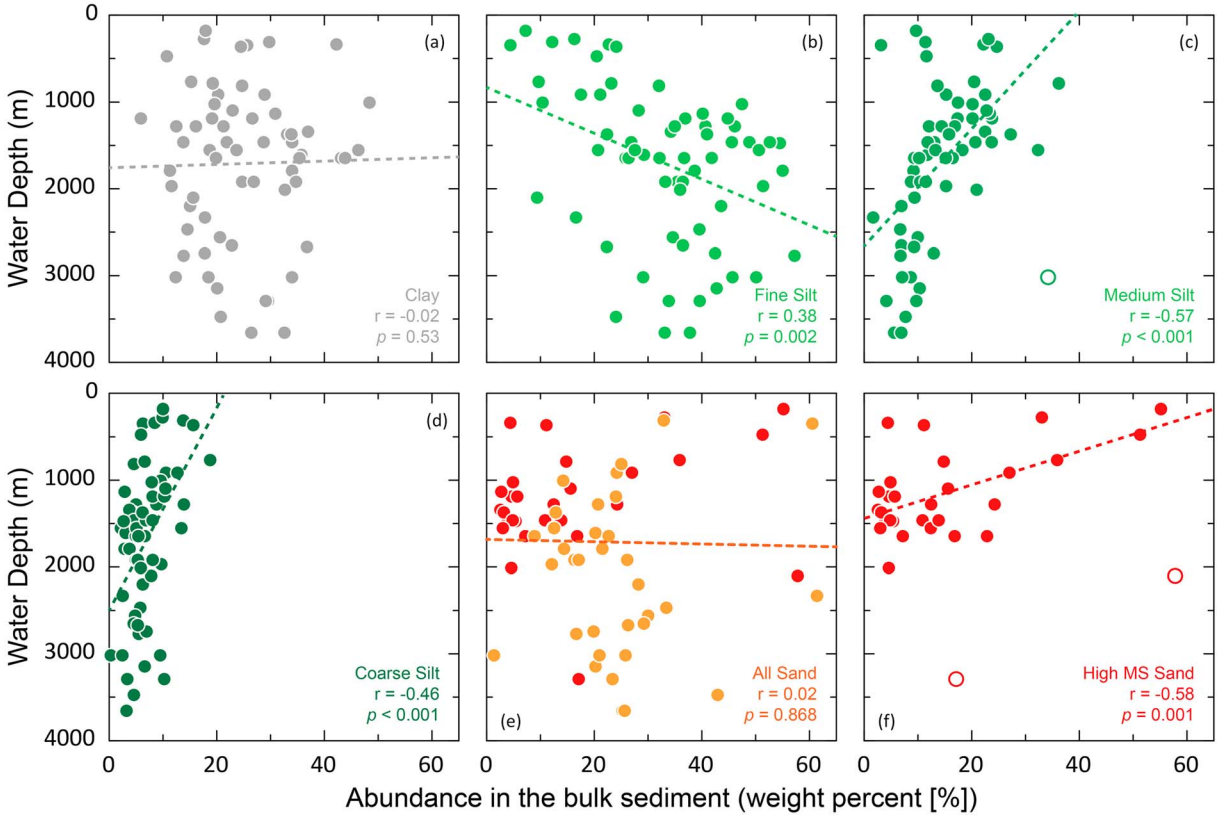

Figure 3. Abundance of (a) clay, (b) fine silt, (c) medium silt, (d) coarse silt, and (e) sand with water depth. Note that the abundance of clay in the cores is independent of water depth while the fine silt fraction abundance increases with water depth. Open circles represent outliers that were not considered in the regression. The negative relationships of medium and coarse silt with water depth indicates restricted transport of these fractions to the deeper Norway Basin. The high magnetic susceptibility lithogenic dominated (f) sand fraction (see text for explanation) follows this same pattern as the medium and coarse silt fractions whereas the biogenic dominated sand fraction (orange symbols in panel e) shows little/no relationship with water depth.

transport-limited framework suggested for the medium and coarse silt fractions with greater abundances in shallow water proximal to potential terrestrial source areas. In contrast the lower MS sand fraction split varies independently of water depth across the full range of water depths as would be expected from an autochthonous biogenic fraction.

4.2. Bulk Magnetic Properties

χ_{HF} values are relatively low compared to bulk MS values (14 times smaller as a median value) so we use bulk MS to provide a first-order approximation of the concentration of ferrimagnetic minerals in the sediment (Thompson & Oldfield, 1986). The median bulk MS value is 1.1×10^{-6} m^3/kg (Interquartile Range [IQR] = 0.71–2.2 $\times 10^{-6}$ m^3/kg) but ranges over an order of magnitude from 0.45–5.9 $\times 10^{-6}$ m^3/kg (Figure 4a). Relatively low MS values (lower quartile = 0.7×10^{-6} m^3/kg) can be found across the full range of water depths, although all sediments recovered deeper than ~2,200 m (n = 19) possess low MS values, aside from one sample at the foot of the Iceland-Faroe sill (core 83; Figure 4a). Relatively high values in the uppermost quartile (>2.2 $\times 10^{-6}$ m^3/kg) are restricted to relatively shallow water depths (<~2,100 m) on the North Iceland shelf, along the Iceland-Faroe Ridge, and at the northern extent of the Iceland Plateau adjacent to Jan Mayen (Figure 4a). These results agree strongly with previous bulk MS results of surface sediments from the Nordic Seas by Pirrung et al. (2002) and Watkins and Maher (2003) who also found high bulk MS values (>2 $\times 10^{-6}$ m^3/kg) in shallow water along the Iceland-Faroe ridge, around Jan Mayen, and on the Iceland shelf.

M_s and M_{rs} are also sensitive to the concentration of ferrimagnetic minerals and mimic the MS values (correlation (r) values of M_s and M_{rs} with MS are 0.99 and 0.97, respectively). The ratio of M_{rs}/M_s is sensitive to variations in ferrimagnetic grain size and Ti-content (Day et al., 1977) with higher values indicative of a finer ferrimagnetic and/or a Ti-rich ferrimagnetic mineral assemblage. Bulk M_{rs}/M_s ratios have a median value of

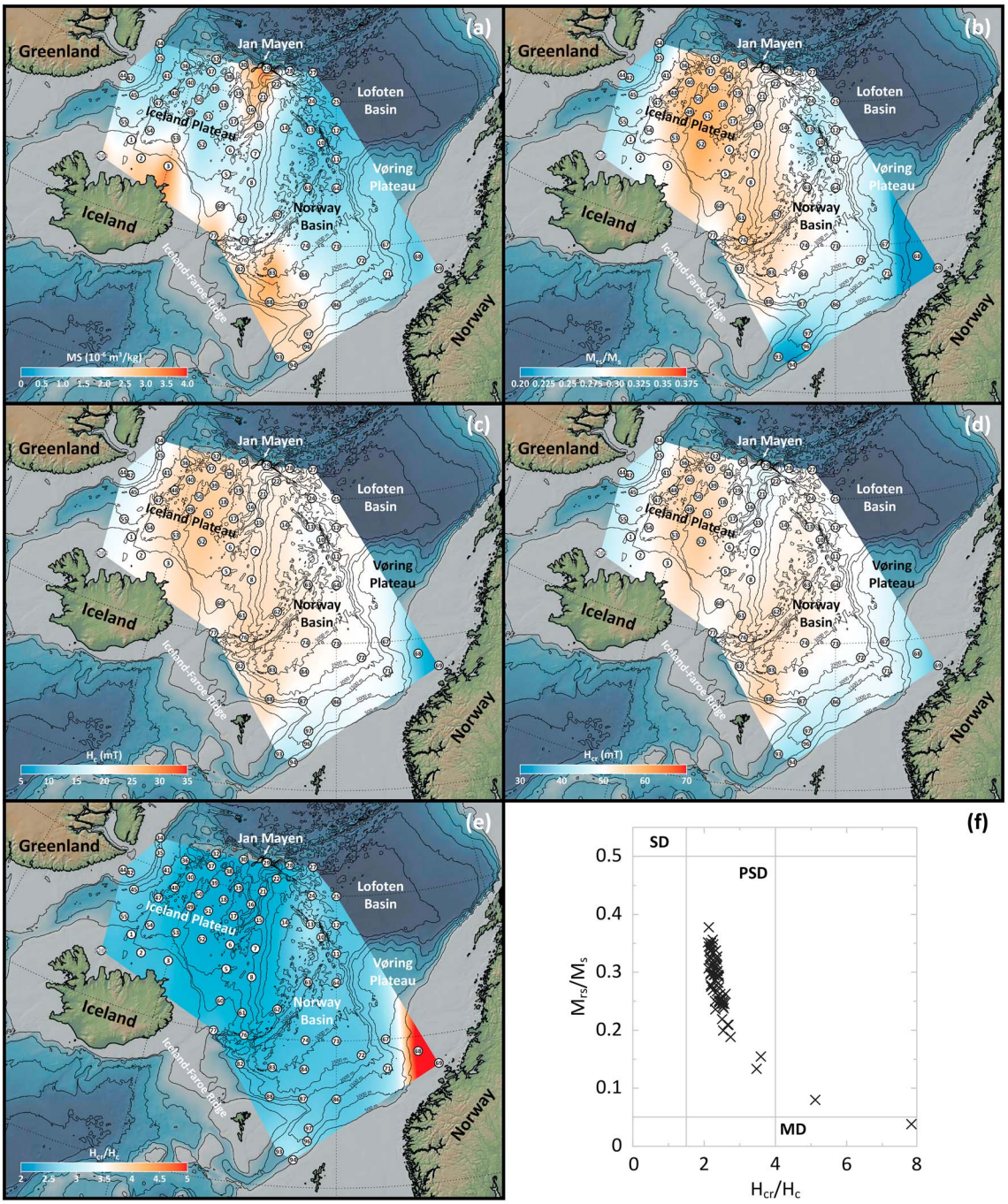

Figure 4. Bulk sediment values of; (a) MS, (b) M_{rs}/M_s, (c) H_c, (d) H_{cr}, (e) H_{cr}/H_c across the Edisto Array. Note the higher concentration of ferrimagnetic minerals around Jan Mayen, Iceland, and along the Iceland-Faroe ridge in panel (a) and the similarity in the spatial patterns of M_{rs}/M_S, H_{cr}, and H_c with higher values across the Iceland Plateau and Norway basin and lower values adjacent to Norway and Greenland. H_{cr}/H_c values are relatively similar across the Edisto Array ranging between ~2 and 3.5; values exceeding this range are only found on the Norwegian margin. (f) Bulk sediment hysteresis parameters H_{cr}/H_c and M_{rs}/M_s shown on a Day Plot (Day et al., 1977). The majority of samples cluster in the PSD region of a Day Plot with M_{rs}/M_s values between 0.186 and 0.378. Four samples have lower M_{rs}/M_s values than this range and possess H_{cr}/H_c values >3 (cores 13, 94, 68, and 69 in order of increasing H_{cr}/H_c values) indicating a coarser ferrimagnetic grain size assemblage. PSD = pseudo-single domain; MD = multidomain; M_S = saturation magnetization; M_{rs} = saturation remanence; SD = Single Domain; Hc = coercivity; Hcr = coercivity of remanence.

0.293 but range over an order of magnitude from 0.038 to 0.378 (Figure 4b). Lowest M_{rs}/M_s values occur on the continental shelves proximal to Greenland, the Faroe Islands, and Norway (Figure 4b). Highest M_{rs}/M_s values occur across the Iceland Plateau and along the western edges of the Norway basin (Figure 4b). Bulk

H_c values (median = 21.3 mT) and H_{cr} values (median = 49.6 mT) follow a similar spatial pattern with the highest values across the Iceland Plateau and western Norway Basin and the lowest values adjacent to Norway, Greenland, and in the Faroe-Shetland Channel (Figures 4c and 4d). Strong correlation between H_c and H_{cr} ($r = 0.89$) suggests that remanence carrying minerals dictate coercivity values and strong agreement between H_c and M_{rs}/M_s ($r = 0.98$) suggests that coercivity is primarily sensitive to the same property that drives the M_{rs}/M_s variability. When M_{rs}/M_s values are combined with H_{cr}/H_c values and viewed on a Day Plot (Day et al., 1977) the core top sediments span the full pseudo-single domain (PSD) and multidomain (MD) regions (Figure 4f). Finer bulk magnetic grain sizes and/or Ti-rich compositions are present across the Iceland Plateau (Figure 4b), while coarser bulk magnetic grain sizes and/or Ti-poor compositions are more common along the margins of Norway and Greenland and in the Faroe-Shetland channel (Figures 4b and 4e).

4.3. Particle Size Specific Magnetic Variability

4.3.1. MS

The clay fraction has the lowest median MS value (0.39×10^{-6} m^3/kg) and the lowest variability in MS values (IQR = 0.27–0.48 $\times 10^{-6}$ m^3/kg) of the five particle size fractions (Figure 5). The strong spatial variability that is observed in bulk MS (Figure 4a) is not evident in the MS values of the clay size fraction (Figure 5a). The median MS value of the medium silt fraction (1.99×10^{-6} m^3/kg) is ~5 times higher than that of the clay fraction, and the coarse silt (median = 1.31×10^{-6} m^3/kg), fine silt (median = 1.01×10^{-6} m^3/kg), and sand fractions (median = 0.82×10^{-6} m^3/kg) all possess median MS values that are ~2–3 times higher than those of the clay size fraction (Figure 5). Lower MS values in the clay size fraction is consistent with previous findings from NNA marine sediments (Hatfield et al., 2016) and terrestrial sediments (Hatfield et al., 2013, 2017) that ferrimagnetic minerals preferentially reside in the silt and sand size fractions. The reason for this consistent observation requires further study, although ferrimagnetic minerals may be better equipped to survive mechanical weathering processes that produce silt and sand size fragments and potentially less able to survive hydrolysis during generation of paramagnetic clay minerals. The spatial variability of MS values in the silt and sand fractions (Figure 5) more closely mimics that of the bulk sediment (Figure 4a). Pirrung et al. (2002) suggested that higher MS in this along the Iceland shelf and Iceland-Faroe ridge resulted from the transport of basaltic grains, rich in ferrimagnetic minerals, as IRD along a counterclockwise surface gyre. An alternate explanation invokes the focusing of bottom currents and greater deposition of entrained lithogenic sediments as currents encounter the Iceland-Faroe ridge and Faroe-Shetland Channel between the Norway basin and the wider NNA Ocean. Regardless of the specific pathway, higher MS values in the silt size fractions (Figure 5), coupled with the similar spatial patterns of silt, sand, and bulk MS (Figures 4 and 5), suggest that these size fractions have a stronger influence on bulk magnetic properties than the clay size fraction.

To examine the contribution that each sediment size fraction makes to the bulk value we exploit the linear additivity of MS and reconstruct bulk MS using equation (1).

$$\chi_{bulk} = f_{>63}(\chi)_{>63} + f_{32-63}(\chi)_{32-63} + f_{10-32}(\chi)_{10-32} + f_{2-10}(\chi)_{2-10} + f_{<2}(\chi)_{<2}, \quad (1)$$

where

χ_{bulk} = the reconstructed MS of the bulk sediment;
f = the fractional abundance of each sediment size fraction (e.g., f_{10-32} is the fractional abundance of the 10–32 μm fraction) with the condition that $f_{>63} + f_{32-63} + f_{10-32} + f_{2-10} + f_{<2} = 1$;
(χ) = MS of each sediment size fraction (e.g., $(\chi)_{10-32}$ is the MS value of the 10–32 μm fraction).

This exercise has two purposes, first it provides a check on the accuracy of the sediment fractionation procedure (as the parts should equal the whole), and second we use it to provide an estimate of the relative importance of each fraction (e.g., medium silt; 10–32 μm) in contributing to the bulk MS value using equation (2).

$$\chi_{cont(10-32)} = \frac{f_{10-32}(\chi)_{10-32}}{\chi bulk} \times 100, \quad (2)$$

where

$\chi_{cont(10-32)}$ = the percentage contribution of the 10–32 μm fraction to bulk MS.

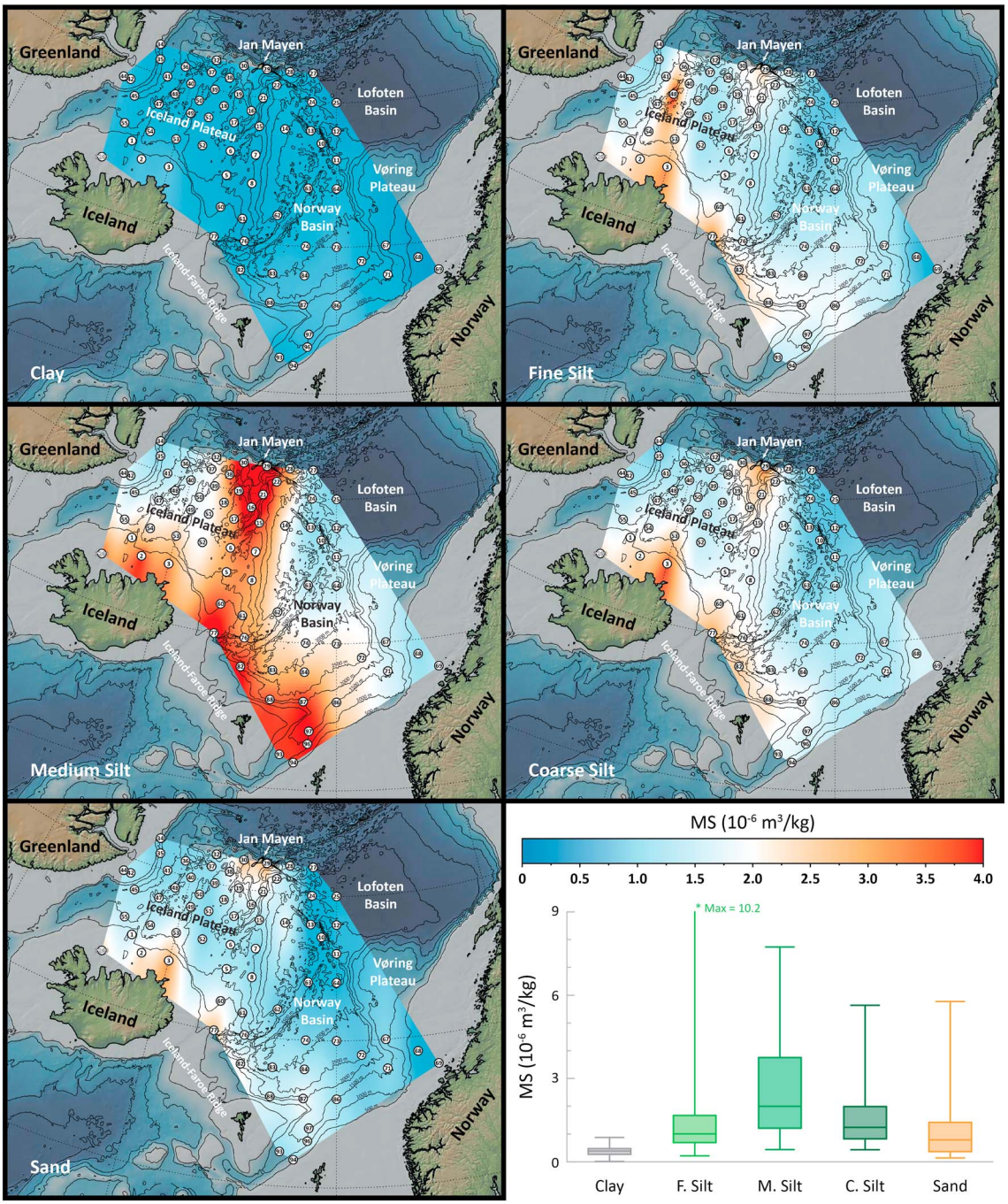

Figure 5. MS values across the Edisto Array for the clay, fine silt, medium silt, coarse silt, and sand size fractions. Also shown are shown are the median (central bar), upper and lower quartiles (box), and maximum and minimum magnetic susceptibility values (bars) for each size fraction (lower right); values that are higher than 4×10^{-6} m^3/kg (the upper range shown in the maps) but lower than the maximum value (upper bar; $n = 9$) are shown as circles. Note the lowest MS values and lowest variability in the clay fraction and highest MS values and greatest variability in the medium silt fraction. Also note the similarity in the spatial distribution of MS through the silt and sand fractions and the lack of this variability in the clay fraction. MS = magnetic susceptibility.

Then, by comparing the abundance of a specific fraction in the bulk sediment (e.g., f_{10-32}) to its contribution to bulk MS (e.g., $\chi_{cont(10-32)}$), we can generate a potency ratio (P-ratio) using equation (3).

$$P\text{–}ratio_{(10-32)} = \frac{\chi_{cont(10-32)}}{f_{10-32\ X\ 100}}. \quad (3)$$

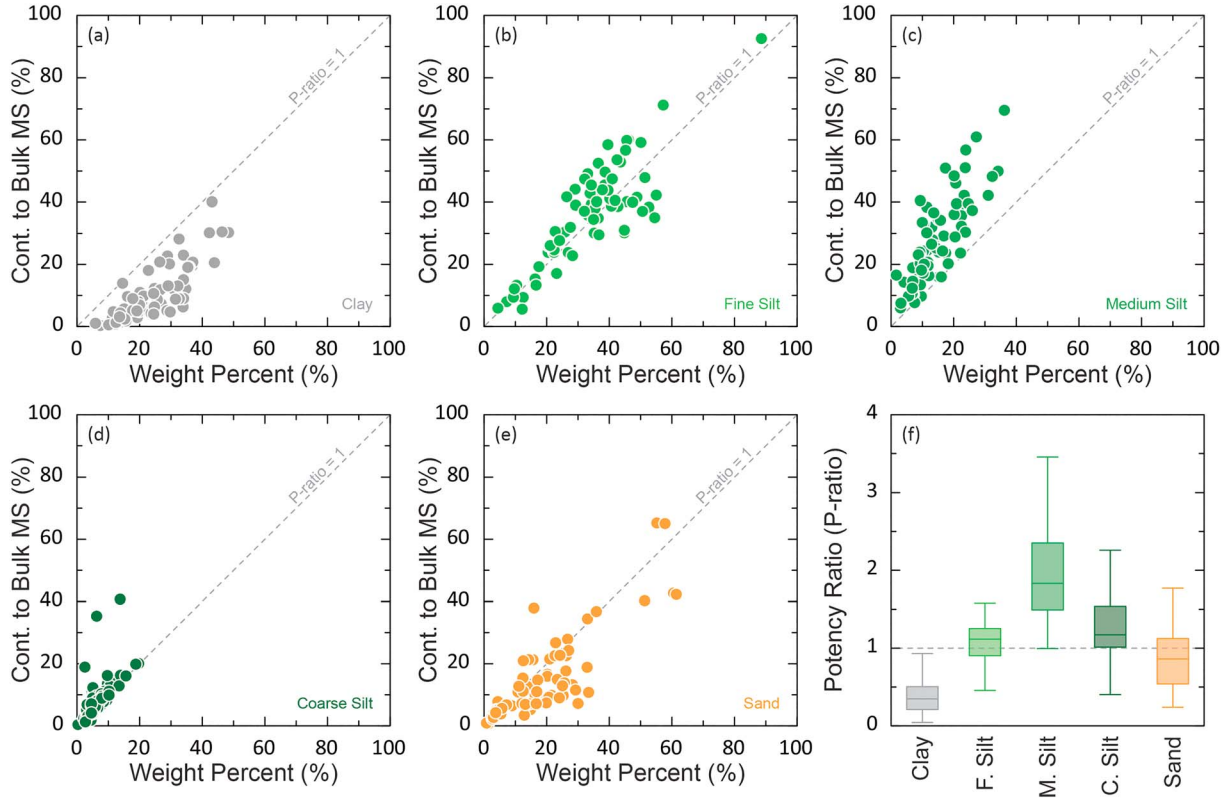

Figure 6. P-ratios for the clay (a), fine silt (b), medium silt (c), coarse silt (d), and sand (e) size fractions. The dashed line follows a PR of 1, samples above the line have P-ratios greater than 1, and samples below the line have P-ratios less than 1. Panel (f) shows box whisker plots summarizing the P-ratio values of the five particle size fractions noting the median, interquartile range, and values 1.5× the interquartile range marking the upper and lower ranges. Note the high P-ratios of the medium silt fraction suggesting that across the Edisto Array medium silts contribute around twice the amount to bulk MS than their abundance suggests. P-ratios = Potency Ratios; MS = magnetic susceptibility.

When the P-ratio is equal to 1 the contribution of that fraction to bulk MS is approximately the same as its physical abundance in the sediment; with a P-ratio > 1 a change in the abundance of that specific fraction will influence bulk MS more than its physical abundance suggests, and a P-ratio < 1 indicates a weaker influence on bulk MS.

The correlation between χ_{bulk} and bulk MS value ($r = 0.97$) demonstrates accurate separation and magnetic measurement of the five different sediment size fractions. Although clay is abundant in the bulk sediment (median = 24%), low clay MS values mean that the clay size fraction only contributes ~9% as a median value (IQR = 5–13%) to bulk MS and its median P-ratio is only 0.35 (IQR = 0.22–0.52; Figure 6). Relatively high abundance of fine silt (median = 35%) coupled with moderately high MS values (Figure 5) and a median P-ratio of 1.11 (IQR = 0.9–1.25; Figure 6) results in ~39% (IQR = 26–45%) of bulk MS being explainable by the fine silt fraction. Although medium silt abundance (median = 13%) is approximately half that of clay and one third that of fine silt, high MS values associated with medium silt (Figure 5) and a median P-ratio of 1.87 (IQR = 1.53–2.37) results in a median contribution of ~25% to the bulk MS value (IQR = 17–37%). The correlation between the abundance of medium silt and bulk MS ($r = 0.67$; not including the 10 sand dominated fractions) is the highest of any of the size fractions, highlighting a strong influence of medium silt on bulk MS values. Median contributions and P-ratios (Figure 6) of the coarse silt ($\chi_{cont(32-63)}$ = ~9% (IQR = 5–11%); P-ratio = 1.18 (IQR = 1.02–1.54)) and sand ($\chi_{cont(>63)}$ = ~11% (IQR = 7–21%); P-ratio = 0.86 (IQR = 0.53–1.05)) fractions are relatively low, generally owing to their relatively low abundance in the bulk sediment. In summary, these median contribution data highlight the importance of fine and medium silt fractions in determining bulk MS values across the Edisto array. High P-ratio values of the medium silt fraction suggests that bulk MS values have greater sensitivity to changes in the abundance of medium silt than any of the other four size fractions (Figure 6).

4.3.2. Hysteresis Properties

The clay size fraction has the highest median M_{rs}/M_s values (0.355) and the lowest variability (IQR = 0.337–0.372) of the five particle size fractions (Figure 7); only three cores have clay M_{rs}/M_s values <0.3 (core 13 at the northern edge of the Norway basin and cores 68 and 69 along the Norway margin). The finest sediment fractions are often the most susceptible to post-depositional alteration, however, the similarity of the Edisto array clay size fractions to terrestrial clays from Iceland (median = 0.336; Hatfield et al., 2017) suggests that authigenic or diagenetic alteration has not significantly affected these sediments. Lower median M_{rs}/M_s values in the fine silt (0.315; IQR = 0.297–0.347) and medium silt (0.257; IQR = 0.22–0.281) fractions reveals a dependence of M_{rs}/M_s with physical grain size (Figure 7) that is mimicked in H_c (Figure 8) and H_{cr} values. The variability in M_{rs}/M_s, H_c, and H_{cr} values also increases with physical grain size from the clay fraction through the coarse silt and sand-size fractions (Figures 7 and 8). However, while the range continues to widen, median M_{rs}/M_s, H_c, and H_{cr} values of the coarse silt and sand fractions increase relative to the medium silt fraction, reversing the trend observed in the finer grain size fractions (Figures 7 and 8).

The highest coarse silt and sand M_{rs}/M_s and H_c values are generally restricted to locations across the Iceland Plateau and within the western Norway basin (Figures 7 and 8); hysteresis properties of cores from these regions are also the least variable with sediment grain size (Figures 7 and 8). The occurrence of potentially submicron sized ferrimagnetic grains (Day et al., 1977; Maher, 1988) in the coarse silt and sand fractions could result from bacterial magnetosomes and/or the trapping of magnetically finer particles within larger biogenic components. However, single domain size bacterial magnetosomes tend to reside in the clay size fraction after sediment fractionation (Hatfield & Maher, 2008) and biogenic contributions are relatively low, if not absent, in the coarse silt size fraction. A similar decoupling of magnetic and physical grain size has been observed in terrestrial sediments from Iceland (Hatfield et al., 2013, 2017). In these samples relatively fine PSD size ferrimagnetic grains are recognized in the silt fraction using Day Plots and FORC diagrams and are imaged as fine-grained titanomagnetite inclusions within larger polycrystalline host grains (Hatfield et al., 2017). Silicate hosted ferrimagnetic inclusions have previously been recognized in marine sediment cores from the North Atlantic Ocean (Hatfield et al., 2016) and the Pacific and Indian Oceans (Chang et al., 2016; Usui et al., 2018). M_{rs}/M_s values are sensitive to magnetic domain state variations (e.g., Day et al., 1977; Dunlop, 1986; Néel, 1955) but also show a strong dependence with magnetite stoichiometry whereby greater titanium substitution yields higher M_{rs}/M_s values for samples of the same size (Day et al., 1977; Roberts et al., 2018). As a result, fine-grained titanomagnetite inclusions have correspondingly higher M_{rs}/M_s values than larger, discrete, stoichiometric magnetite grains (e.g., Roberts et al., 2018). Given the relatively high M_{rs}/M_s values associated with coarse silts and sands across the Iceland Plateau and Norway Basin (Figure 7) and their similarity to Iceland terrestrial samples both in terms of hysteresis parameters and LTMS (see section 4.3.4), we suggest that ferrimagnetic minerals in these cores also exist as titanomagnetite inclusions. This interpretation reconciles the presence of PSD size grains in the silt and sand size fractions and, as these fractions are more transport limited (Figure 3), explains the occurrence of higher M_{rs}/M_s values across the Iceland Plateau and western edge of the Norway Basin.

Cores from the margins of Greenland and Norway, from the Faroe-Shetland Channel and from the Lofoten Basin, generally have lower silt and sand M_{rs}/M_s and H_c values than those from the Iceland Plateau and Norway Basin (Figures 7 and 8). In cores from these locations, for example, cores 34 and 35 (on the Greenland shelf) and cores 68 and 69 (proximal to Norway), M_{rs}/M_s values continue to decrease with increasing physical grain size, reaching minimum M_{rs}/M_s values of ~0.03 in cores 68 and 69 (Figure 7). This trend is largely mimicked in H_c (and H_{cr}) with the largest coercivity decreases occurring between the fine silt and medium silt fractions (Figure 8). These samples show similar behavior (see section 4.3.4) to terrestrial Greenlandic samples that are composed of discrete grains of near-stoichiometric magnetite (Hatfield et al., 2013, 2017), leading us to suggest a similar mineralogy of these Greenland proximal Edisto cores. Samples from cores proximal to Norway display a similar pattern, and, although we have not directly examined terrestrial samples from Norway, studies of proximal marine sediment cores suggest sediments in this region are sourced from the Norwegian margin and are delivered by bottom currents (Dahlgren et al., 2003; Halvorsen, 1974; Newton & Huuse, 2017; Worm, 2016).

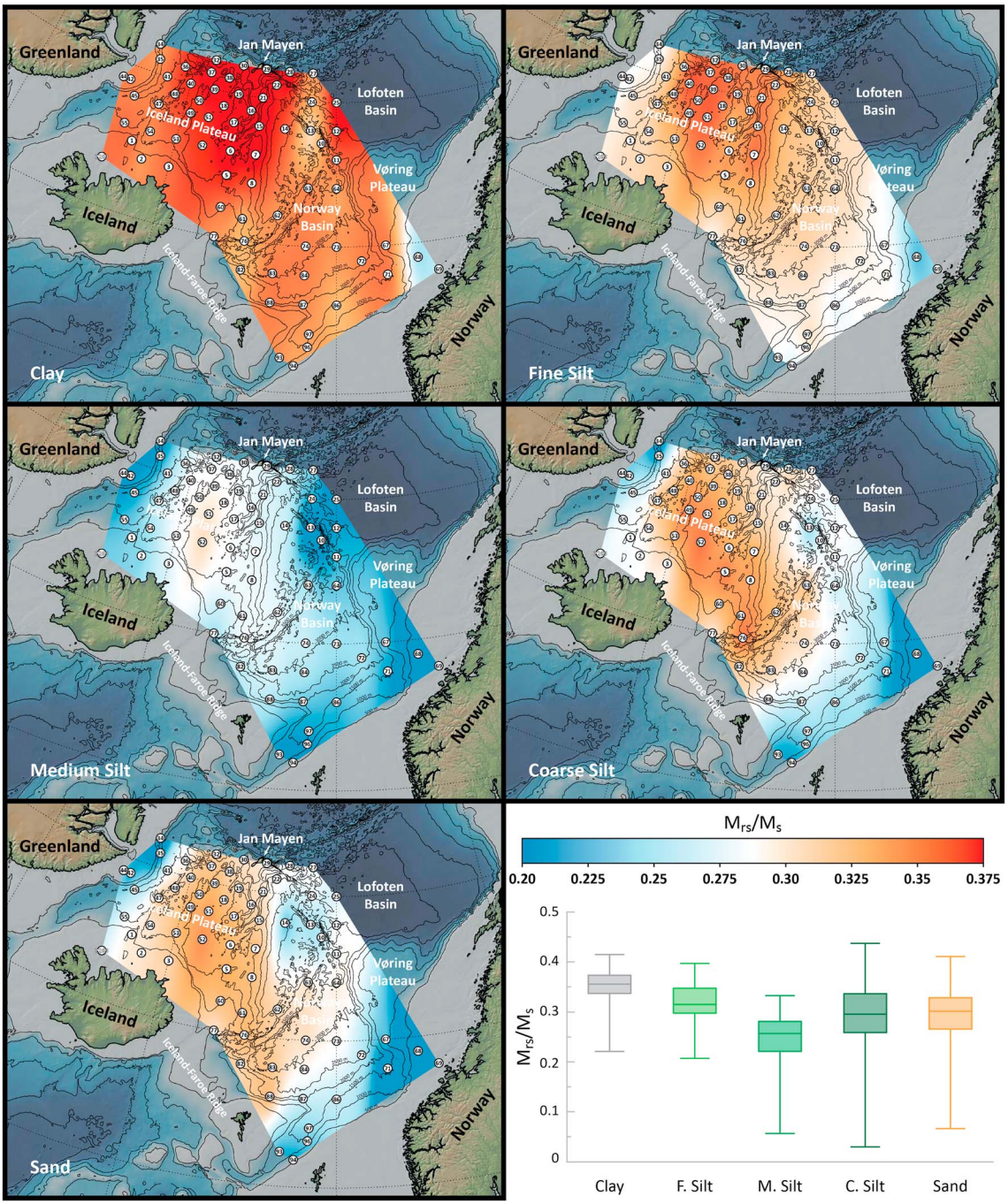

Figure 7. M_{rs}/M_s values across the Edisto Array for the clay, fine silt, medium silt, coarse silt, and sand size fractions (maps). Also shown are shown are the median (central bar), upper and lower quartiles (box), and maximum and minimum magnetic susceptibility values (bars) for each size fraction (lower right); values that are outside of the range depicted in the interpolations (0.2–0.4) but within the maximum and minimum values (bars; $n = 36$) are shown as circles. Note that the clay size fraction has the highest M_{rs}/M_s values and the lowest variability. Variability increases with increasing physical size with locations across the Iceland Plateau and in the Norway basin retaining relatively high M_{rs}/M_s values compared to those proximal to Norway and Greenland that have lower values of M_{rs}/M_s with increasing physical grain size. M_S = saturation magnetization; M_{rs} = saturation remanence

4.3.3. FORCs

FORCs of four medium silt fractions from the Iceland Plateau (cores 39 and 52), from close to Jan Mayen (core 29), and from the Norway basin (core 74) are characterized by an oval, sometimes truncated, closed-contour intensity structure (Figure 9). Triangular contour lines intersect with the vertical axis and are indented on the lower branch indicating populations of PSD sized grains (Roberts et al., 2000). Peak

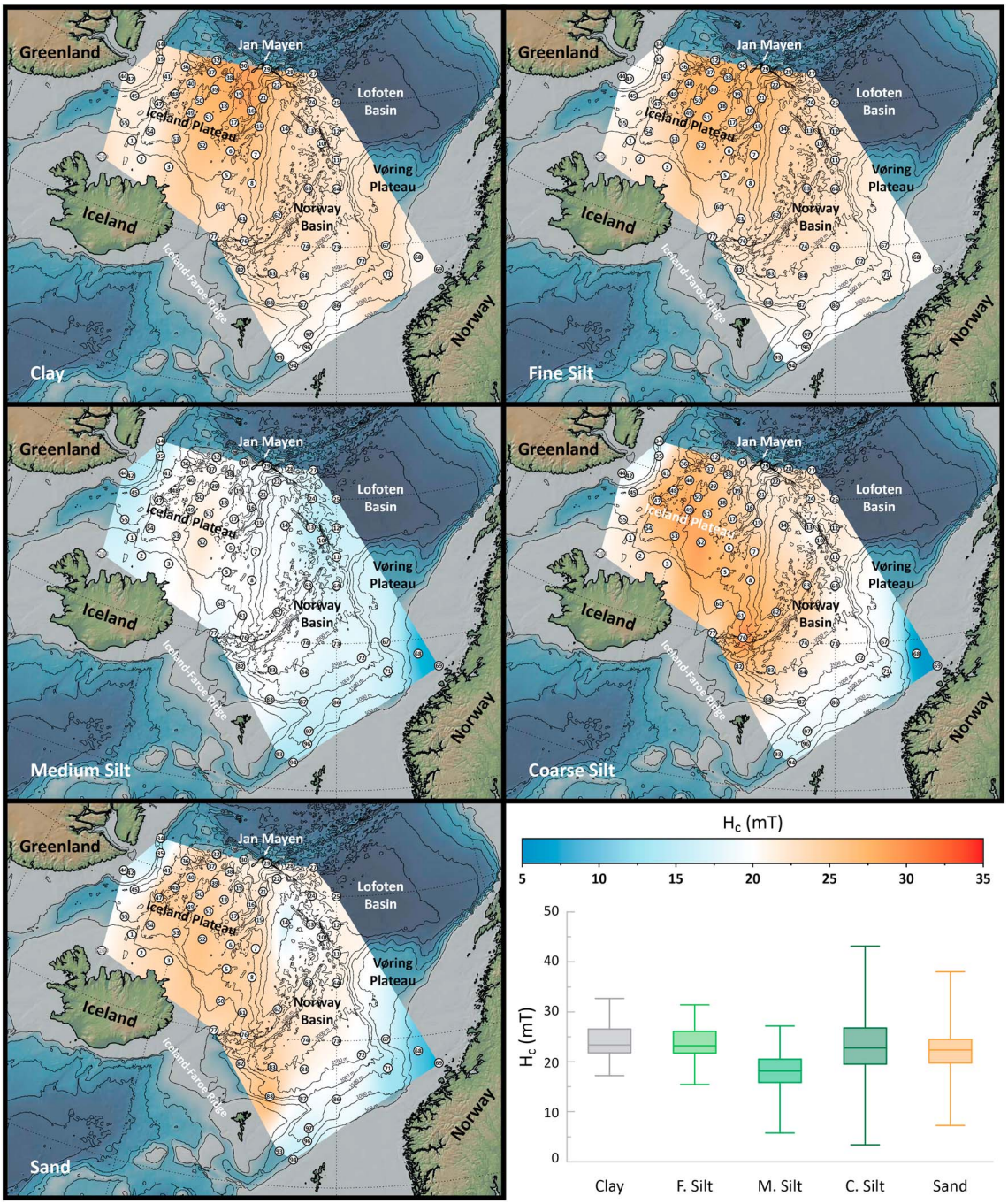

Figure 8. H_c values across the Edisto Array for the clay, fine silt, medium silt, coarse silt, and sand size fractions (maps). Also shown are the median (central bar), upper and lower quartiles (box), and maximum and minimum magnetic susceptibility values (bars) for each size fraction (lower right). Note that the clay size fraction has the highest H_c values and the lowest variability similar to the M_{rs}/M_s data. Variability increases with increasing physical size with locations across the Iceland Plateau and in the Norway basin retaining relatively high H_c values compared to those proximal to Norway and Greenland that have the lowest values of H_c.

coercivities are lower than those typical of bacterial magnetosome compositions (e.g., Channell et al., 2016; Ludwig et al., 2013) which are likely to reside in the finer sediment fractions and the shape and structure of these four medium silt size FORCs resemble those of terrestrial Iceland silts reported in Hatfield et al. (2017). The intensity structure of Core 52 extends further along the H_c axis and has higher M_{rs}/M_s values (Figure 7) than cores 29, 39, and 74 suggesting a slightly finer magnetic grain size assemblage (Figure 9). Core 44 on the

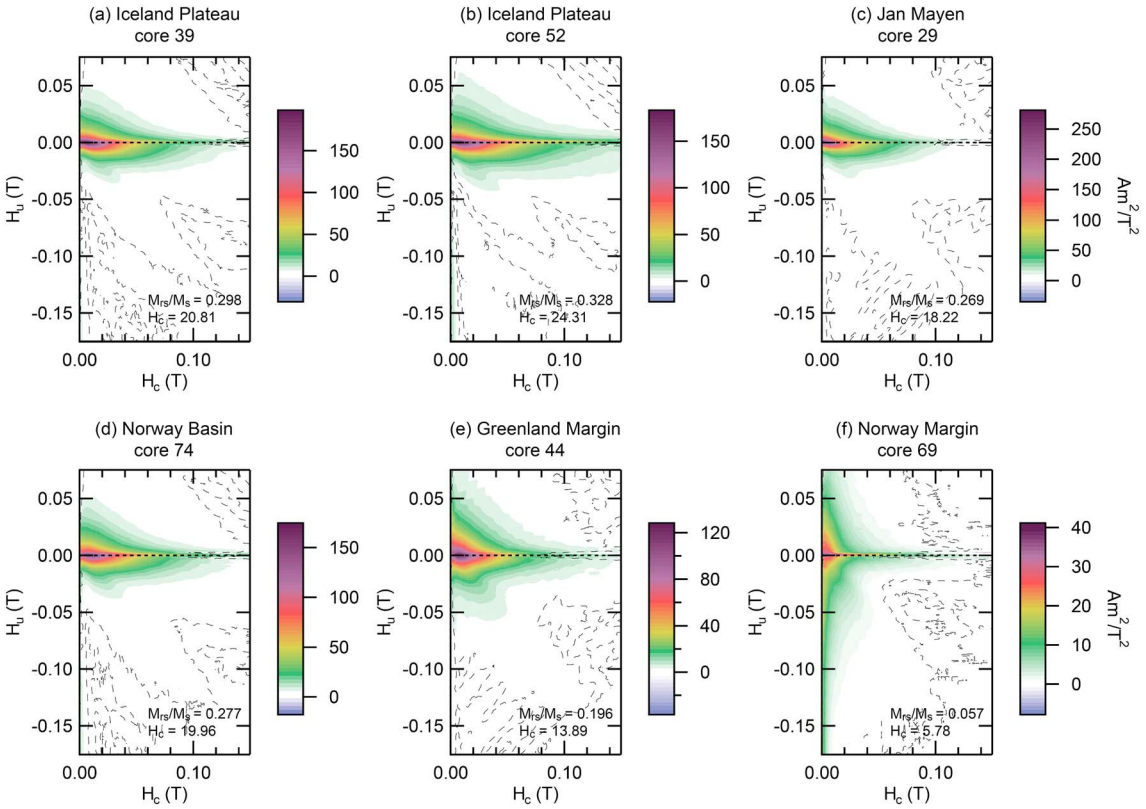

Figure 9. FORC diagrams of medium silt fractions from the Iceland Plateau (a–b), proximal to Jan Mayen (c), the Norway Basin (d), and close to the margins of Greenland (e), and Norway (f). FORCs were processed using VARIFORC (Egli, 2013) smoothing (Sc0 = 4, Sb0 = 3, Sc1 = 7, Sb1 = 7, horizontal and vertical $\lambda = 0.1$) in FORCinel 3.0 (Harrison & Feinberg, 2008). Dashed lines indicate regions of the FORC distribution significant at the 0.05 level. M_{rs}/M_s and H_c values were determined from the major hysteresis loop. FORC = First-order reversal curve; M_S = saturation magnetization; M_{rs} = saturation remanence.

Greenland margin also exhibits a PSD type structure, but lower peak coercivity, a more pronounced lower branch lobe, and greater spread along the H_u axis suggests a coarser assemblage of magnetic grains than those found across the Iceland or Norway Basins. The intensity structure of core 69 is spread vertically along the H_u axis indicating a MD grain size assemblage (Roberts et al., 2000). Similarity of FORCs from cores 44 and 69 to FORCs measured on discrete silt-size magnetite from Greenland (Hatfield et al., 2017) suggests that samples proximal to the Norwegian and Greenlandic margins are magnetically coarser than those recovered from across the Iceland Plateau.

4.3.4. Low Temperature MS

The medium silt LTMS profile of core 69 (proximal to the Norwegian margin) is characterized by a large increase in MS from ~100 K to peak values ~130 K associated with the Verwey transition in stoichiometric magnetite (Moskowitz et al., 1998; Özdemir et al., 1993). Similar to core 69, cores 10 and 25 located close to the Lofoten Basin, and core 34 on the Greenland shelf, have MS values that peak at ~130 K and decrease with increasing temperature (Figure 10). The remaining 17 profiles are characterized by a range of concave up MS profiles above ~175 K that resemble a range of titanomagnetite compositions and titanomagnetite and magnetite mixtures (e.g., Hatfield et al., 2017; Moskowitz et al., 1998). If we interpret these normalized MS profiles in terms of magnetic mineralogy following Hatfield et al. (2017) then the data in Figure 10 suggest that a mixture of magnetite and Ti-poor and Ti-rich titanomagnetite dominate the ferrimagnetic mineral assemblage of sediments recovered from across the Greenland and Norwegian Seas.

By comparing these 21 normalized LTMS medium silt profiles to a stoichiometric magnetite dominated Greenlandic terrestrial silt endmember (EM) and a Ti-rich titanomagnetite dominated Icelandic terrestrial silt EM (Hatfield et al., 2017; Figure 10c) we can estimate the relative mixing of magnetite and

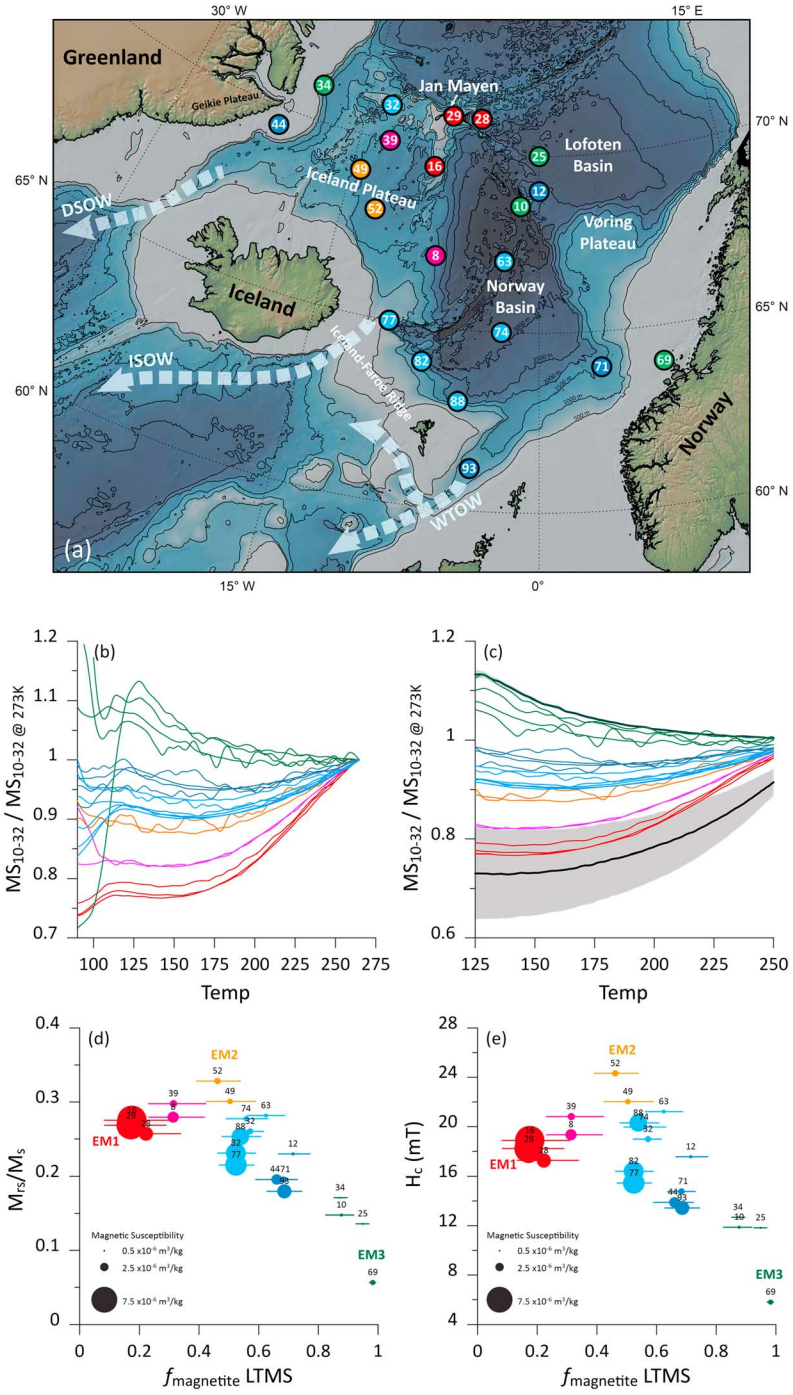

Figure 10. (a) Map of the subset of samples selected for measurement of LTMS. Core locations are colored by their endmember affiliation (see text and panels d and e). (b) Normalized LTMS profiles for the 90–273 K temperature range (colored as per panels d and e). (c) the same LTMS profiles as panel b for the 125–250 K temperature range shown alongside the Greenland (thicker green line) and Iceland (thicker black line) terrestrial endmembers from Hatfield et al. (2017), shading is two standard deviations around the mean endmember value. (d–e) Median fraction magnetite of the LTMS profiles calculated by unmixing the contributions of the terrestrial endmembers in panel (c) shown alongside M_{rs}/M_s (d) and H_c (e) the spread is the interquartile range around the median value. The size of the symbols reflects the MS value of the core and the colors help identify three distinct endmembers (EM1 red; EM2 orange; EM3 green) and mixtures of those endmembers (pink, light blue, dark blue) in varying proportions. DSOW = Denmark Strait Overflow Water; ISOW = Iceland Scotland Overflow Water; WTOW = Wyville Thompson Overflow Water; EM = endmember; MS = magnetic susceptibility; LTMS = low temperature dependence of MS; M_S = saturation magnetization; M_{rs} = saturation remanence.

titanomagnetite sources. We present this data as the fraction of magnetite (f_{mag}) using equation (4) following Hatfield et al. (2017):

$$f_{mag} = \left(C \times \left[\left(R_{edisto} - R_{mag}\right)/\left(R_{titano} - R_{edisto}\right)\right] + 1\right)^{-1}, \quad (4)$$

where

C = the ratio of the Magnetite EM concentration to the titanomagnetite EM concentration (using $\chi_{273\ K}$);

R = χ/χ_{273K} of each Edisto sample (R_{edisto}), magnetite EM (R_{mag}), and titanomagnetite EM (R_{titano}).

To quantify uncertainty, we solve for f_{mag} 10,000 times, varying our choice of C, R_{mag}, and R_{titano} each time based on the terrestrial MS values and χ/χ_{273K} profiles in Hatfield et al. (2017). For each iteration the f_{mag} estimate is the median value of 126 equally spaced f_{mag} estimates over the 125–250 K temperature range. Uncertainty in f_{mag} is presented as the IQR surrounding the median f_{mag} value in Figures 10d and 10e.

The Edisto samples span the entire terrestrial EM space (Figure 10c) and when f_{mag} is plotted against hysteresis parameters (Figures 10d and 10e) the spread of data can be best described by the existence and mixing of three distinct EMs. We add a third dimension to these plots by scaling the size of the datapoints by their MS values. Endmember 1 (EM1) is characterized by relatively high concentrations of Ti-rich titanomagnetite and relatively high M_{rs}/M_s and H_c values and is most abundant in the cores proximal to Jan Mayen (cores 16, 28, and 29; red data in Figure 10). EM2 has the highest M_{rs}/M_s and H_c values and is characterized by higher contributions of fine-grained magnetite and/or Ti-poor titanomagnetite relative to EM1. Two Iceland proximal cores on the Iceland Plateau (cores 49 and 52; orange data in Figure 10) are dominated by EM2 (Figures 10d and 10e). EM3 is distinguished by its low M_{rs}/M_s and H_c values and the dominance of magnetite. Core 69 from the Norway margin is typical of EM3, but cores from the Lofoten Basin (cores 10 and 25) and from the Greenland margin (core 34) are strongly influenced by contributions of EM3 (green data in Figure 10).

The spatial distribution of these three EMs (Figure 10a) points to Ti-rich (EM1) and Ti-poor (EM2) titanomagnetite sources from Jan Mayen and Iceland, respectively, and a magnetite dominated source located along the margins of Greenland and Norway (Figure 10a). FORC diagrams and relatively high M_{rs}/M_s values of EM1 and EM2 dominated samples suggest that titanomagnetites from both sources are hosted as fine-grained inclusions within the silt-size fraction. In contrast, the FORC diagram of core 69 and the lower M_{rs}/M_s values of EM3 suggests that EM3 magnetites likely exist as discrete entities. The grouping of Norway and Greenland proximal samples supports the inferences from hysteresis and FORC data that samples from Norway and Greenland have similar compositions. These EMs are also consistent with hysteresis and FORC data acquired on terrestrial glacio-fluvial sediments from Iceland and Greenland (Hatfield et al., 2017). Geological variability of these regions likely dictates the variance in magnetic properties and the mixing of these three mineralogical EMs likely controls magnetic properties across the basin. For example, cores 8 and 39 (pink data in Figure 10) are located on the central and eastern edges of the Iceland Plateau proximal to both Jan Mayen and Iceland and fall on a mixing line of EM1 and EM2. The remaining 10 profiles fall as intermediaries of all three EMs. Cores 12, 44, 71, and 93 (dark blue data in Figure 10) are distinguishable from cores 32, 63, 74, 77, 82, and 88 (light blue data in Figure 10) by their higher EM3 contributions. These cores are located around the margins of the basin and are closer to the Greenland, Norway, and Faroe margins than Iceland and Jan Mayen explaining the greater influence of EM3. The remaining cores largely occupy locations in the Norway basin (cores 63 and 74) and along the Iceland-Faroe ridge (cores 77, 82, and 88) and likely receive inputs from all three source regions. The higher MS values of cores 77, 82, and 88, and core 93 from the Faroe-Shetland channel, could result from contributions of EM1, however, if this was a significant source of ferrimagnetic minerals we would then also expect cores 8 and 39 to also have high MS values. Similarly if the high MS of these cores resulted from a clockwise surface gyre delivering icerafted material from Iceland and the volcanics of East Greenland we might expect them to contain higher EM2 contributions. Instead it is more likely that the higher MS values of cores along the base of the Iceland-Faroe ridge results from transport of lithogenic sediment in bottom currents from all three source regions and their accumulation in this region as currents are forced to slow and climb the submarine sill.

5. Discussion

5.1. The Influence of Sediment Texture and Sediment Source on Bulk Magnetic Properties

Magnetic concentration and magnetic grain size of surface sediments across the southern Greenland and Norwegian Seas are strongly particle size and sediment source dependent. The clay size fraction is ubiquitous across the region (Figures 2 and 3), but is the least variable both in terms of magnetic concentration and coercivity (Figures 5, 7, and 8) and has the smallest influence on bulk magnetic properties (Figure 6). The silt-size fractions possess higher concentrations of ferrimagnetic minerals (Figure 5) and the medium silt size fraction exerts the greatest influence on bulk MS values (Figure 6). The noncohesive (>10 μm) fractions are more transport limited than the cohesive (<10 μm) fractions (Figure 3) and these coarser fractions contain the greatest spatial variability in magnetic properties (Figures 5, 7, and 8). This variability can be best explained by the mixing of three distinct EMs within a source-proximal transport-limited framework (Figure 10). Fine-grained titanomagnetites of varying compositions form two EMs that dominate the sediments proximal to Iceland and Jan Mayen and mixtures of these two sources dominate the ferrimagnetic properties across the Iceland Plateau. Core sediments located along the margins of Greenland and Norway are dominated by proximally sourced discrete detrital magnetite. While these cores are from two geographically distinct regions, magnetically they are similar, and form the third EM. Cores from the Lofoten Basin have high EM3 contributions, likely from inputs of similarly coarse grained magnetite from the Northern Norwegian margin that are transported southward into the Edisto Array by bottom currents. Finally the sediments in the Norway Basin and along the Iceland-Faroe ridge appear to be a mixture of both Iceland Plateau and Norwegian margin/Lofoten Basin sources.

Spatial and textural variability in magnetic concentration, magnetic mineralogy, and magnetic grain size within surface sediment fractions across the Edisto array is not surprising given the heterogeneity in the geology that frames the Greenland and Norwegian Seas. However, these results challenge the widely held view of a relatively common, homogenized, basaltic sediment source area that stretches from the margins of Greenland to the Faroe Islands and Norway. Moreover, these first observations of the strong dependence of magnetic properties with sediment particle size and sediment source have important implications for the interpretation of the bulk magnetic records. For example, these data suggest that temporal variations in magnetic concentration (and magnetic grain size) that were thought to depend solely on changes in the delivery of discrete ferrimagnetic grains can potentially be driven by changes in the sediment texture (and sediment source) at any site.

In order to better evaluate the influence that sediment texture can have in driving bulk magnetic variation we manipulate the abundance of different fractions in the bulk sediment (the f terms in equation (1)) and model the resulting bulk MS and M_{rs}/M_s values (Figure 11). For each core sample we use the existing textural composition as the initial condition (iteration 0) and then progressively alter the sediment texture four times (iterations 1–4), under two scenarios. For scenario 1 we coarsen the average sediment texture of the sample by increasing the existing proportions of medium silt (+25%), coarse silt (+10%), and sand (+2.5%) relative to fine silt (−12.5%) and clay (−25%) for each iteration (Figure 11a). Under scenario 2 we fine the average sediment texture by increasing the existing proportions of clay (+25%) and fine silt (+15%) and decrease the proportions of medium silt (−5%), coarse silt (−15%), and sand (−20%) for each iteration (Figure 11b). The relative changes in sediment composition under these two scenarios are not intended to replicate specific processes that can drive texture changes (e.g., gravity flows, mass movements, changes in bottom current strength, terrestrial fluxes, or IRD delivery) but instead provide an estimation of the sensitivity of bulk magnetic properties to a doubling (after four iterations) of medium silt (scenario 1) or clay (scenario 2) that could result from the influence of any of these processes.

The results of all 71 core samples are shown in the eight panels of Figure 11 as thin gray lines. The 21 samples used to derive the three EMs in Figure 10 are highlighted in Figure 11 using thicker lines and the same color scheme. A coarsening of the average sediment texture under scenario 1 results in a median increase in bulk MS values of 33% (IQR = 20–47%; Figures 11c and 11d). Fining of the average sediment texture under scenario 2 results in a decrease in the median MS value by −12% (IQR = −19% to −4%; Figures 11g and 11h). The greater change in MS values in response to scenario 1 compared to scenario 2 results from the higher P-ratio of medium silt compared to the other fractions (Figure 6). Increases in MS under scenario 2 (Figure 11h) is restricted to 12 cores and occurs because of the relatively large net increase of fine silt with

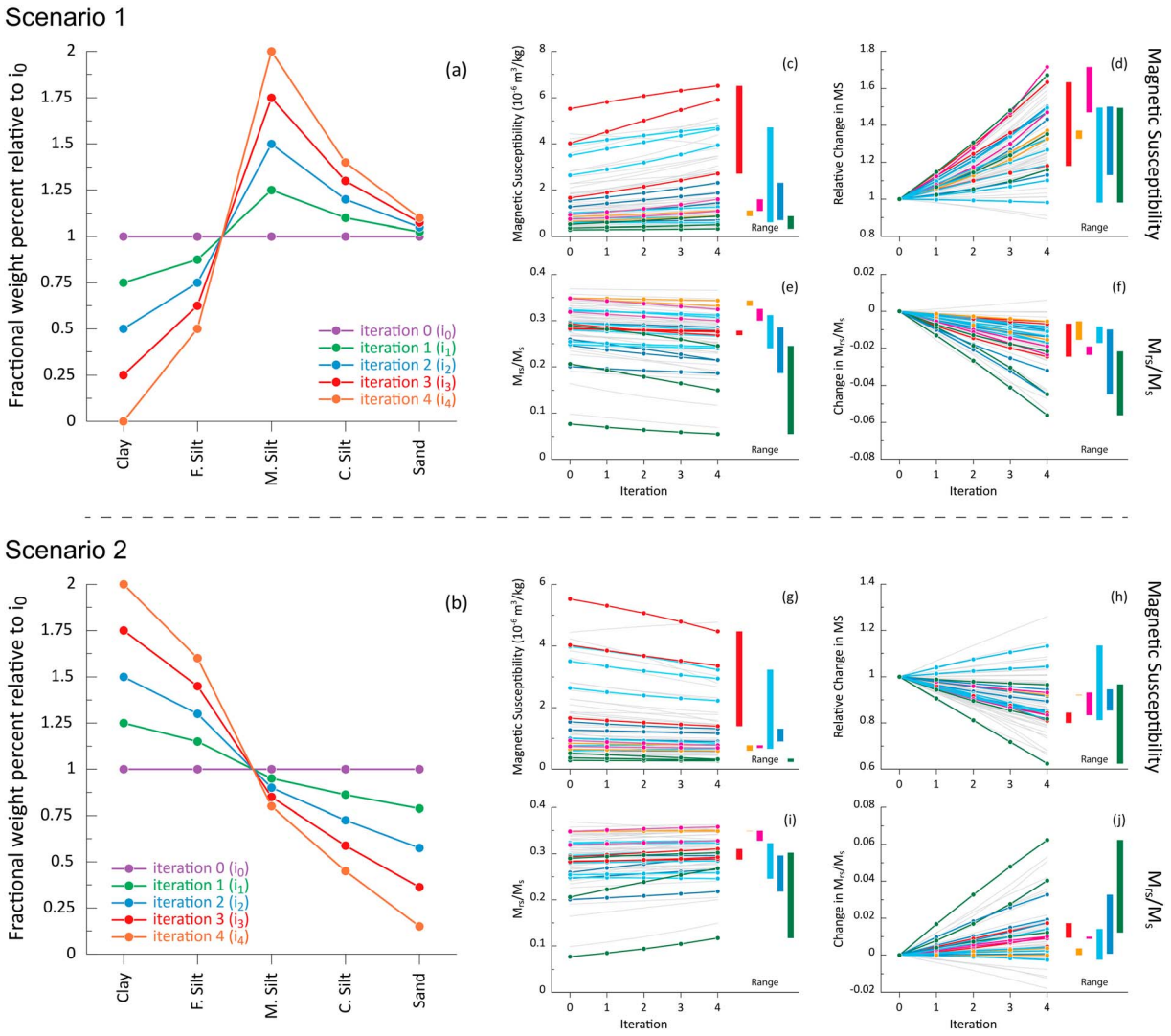

Figure 11. (a and b) Sediment texture changes relative to the existing composition of each core (iteration 0; i_0) for each iteration (i_1–i_4) under scenario 1 (a) and scenario 2 (b). The average sediment texture increases under scenario 1 and decreases under scenario 2. The resulting bulk MS (c and g) and M_{rs}/M_s (e and i) values and relative change in MS (d and h) and absolute change in M_{rs}/M_s (f and j) for each core after each iteration are shown as gray lines. The same 21 cores as used in Figure 10 are highlighted here using the same color scheme to highlight the spatial variability across the Edisto Array. In general bulk MS increases under scenario 1 (d) and decreases under scenario 2 (h) across all endmembers with little/no spatial bias or tendency in the relative amount or direction of change. In contrast M_{rs}/M_s values show a strong spatial imprint with EM3 more strongly susceptible to texture changes compared to EM1 and EM2 (panels f and j). M_S = saturation magnetization; M_{rs} = saturation remanence.

relatively high MS values in these cores (Figure 11b). MS sensitivity to texture does not appear to exhibit any spatial pattern (bars in Figures 11d and 11h) suggesting that bulk MS variability can be strongly influenced by changes in sediment texture across the entire region.

Bulk values of M_{rs} and M_s are derived independently using equation (1) and then combined to generate bulk M_{rs}/M_s value estimates under both scenarios. M_{rs}/M_s values generally decrease under scenario 1 and increase under scenario 2 (Figures 11e–11f) and likely reflect the physical grain size dependence of M_{rs}/M_s (Figure 7). However, unlike MS variability, the M_{rs}/M_s values of each EM grouping possesses a strong spatial imprint. EM1 and EM2 dominated cores (warmer colors in Figures 11e and 11i) across the Iceland Plateau have the highest M_{rs}/M_s values but are relatively insensitive to sediment texture changes with an average decrease of 0.01 under scenario 1 (Figure 11f) and an average increase of <0.01 under scenario 2 (Figure 11j) after four iterations. This insensitivity to sediment texture changes likely results from the included nature of titanomagnetites within larger host grains in EM1 and EM2 dominated samples that

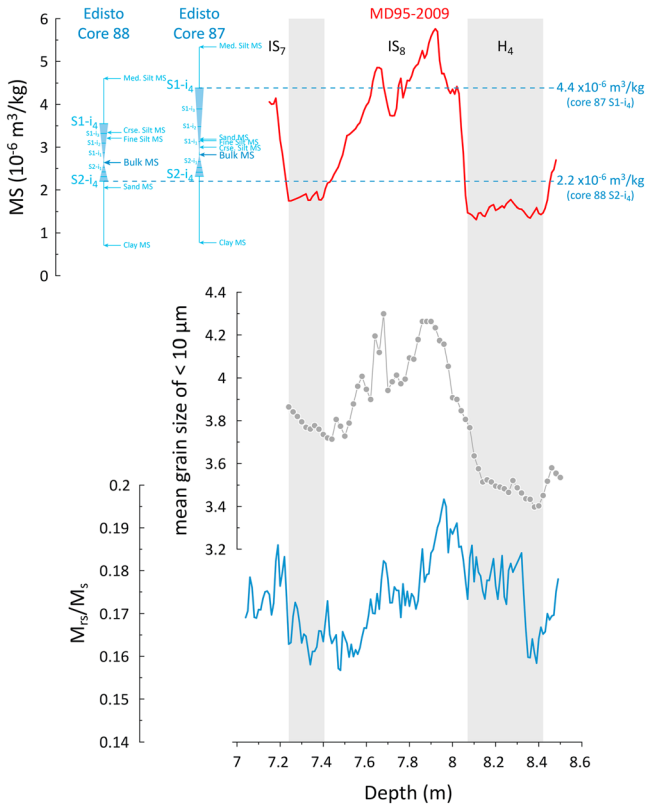

Figure 12. (a) MD95-2009 bulk MS (red), average size of the <10 μm fraction (gray), and bulk M_{rs}/M_s (dark blue) from Heinrich Event 4 (H_4) to D-O interstadial 7 (IS_7); all data from Ballini et al. (2006). Shown alongside the MD95-2009 bulk MS data are the bulk and particle size MS values for Edisto cores 88 and 87 and the modeled bulk MS value after four iterations under scenario 1 (S1-i_4) and scenario 2 (S2-i_4) (light blue). The minimum and maximum values under these scenarios from these cores are traced over the bulk MD95-2009 data (dashed light blue lines) to highlight the potential range of MS values in MD95-2009 that could be driven by texture variations. MS = magnetic susceptibility; M_S = saturation magnetization; M_{rs} = saturation remanence.

effectively reduces the sensitivity of magnetic grain size to physical grain size changes. In contrast, the bulk M_{rs}/M_s values of EM3 samples proximal to Norway and Greenland exhibit greater sensitivity to sediment texture variations with increases and decreases in M_{rs}/M_s values up to 0.06 after four iterations under scenarios 1 and 2, respectively (Figures 11f and 11j). This increased variability results from the greater range of discrete ferrimagnetic grain sizes in EM3-dominated sources that can sort and scale with physical grain size to a greater extent than EM1 and EM2 sources. EM mixtures (light blue, dark blue, and pink data in Figure 11) fall as intermediaries of their respective EMs with cores that possess slightly higher EM3 contributions (dark blue data in Figure 11) having lower M_{rs}/M_s values and greater M_{rs}/M_s variability than those with lower EM3 contributions (light blue and pink data in Figure 11). While the spatial variability in M_{rs}/M_s values is strongly heterogeneous and dominated by proximity to different EM sources, only EM3 (Greenland and Norway Proximal) sources display strong sensitivity to variations in sediment texture, a finding previously inferred in the NNA by Hatfield et al. (2013) using only a terrestrial data set.

5.2. Understanding Bulk Magnetic Property Variability Across the Nordic Seas

A relationship between MS variations and temperature in Greenland ice cores has been observed in drift deposits north and south of the sills separating the Nordic Seas from the NNA basins (e.g., Ballini et al., 2006; Kissel, 2005; Kissel et al., 1999; Moros et al., 1997; Rasmussen et al., 1996, 1997). This relationship assumes that changes in the strength of bottom currents are in phase with Greenland temperature (e.g., Bianchi & Mccave, 1999; Elliot et al., 2002; Stoner et al., 2000) and that hydrodynamic variations mediate the transport, and ultimately the delivery, of ferrimagnetic grains. For four cores that exhibit this behavior within our study area (Figure 1), bulk MS varies over a factor of 3–8 during Marine Isotope Stage 3 (57–29 ka; Lisiecki & Raymo, 2005) excluding the MS lows associated with Heinrich stadials (Kissel et al., 1999; Rasmussen et al., 1996). Cores MD95-2009 and ENAM93-21 are in approximately the same location, positioned just north of the Faroe-Shetland channel, core MD95-2010 is on the Vøring Plateau close to the Norwegian margin, and core PS2644-5 is just north of the Iceland shelf, close to the Denmark Strait (Figure 1).

The magnetic and geochemical properties of core MD95-2009 through Dansgaard-Oeschger interstadial 8 were studied in detail by Ballini et al. (2006; Figure 12). The median MS value through this interval (2.8×10^{-6} m^3/kg) is similar to the bulk MS values of the proximal Edisto cores 87 (2.8×10^{-6} m^3/kg) and 88 (2.6×10^{-6} m^3/kg; Figure 12). By manipulating the sediment texture of these two samples under scenarios 1 and 2 (resulting range = 2.2–4.4 $\times 10^{-6}$ m^3/kg), we show that ~50% of the bulk MS variability observed in MD95-2009 could be explained by texture variations of the existing sediment (Figure 12). To explain the rest, either the absolute amount of ferrimagnetic grains in transport must change, or the source of the sediment must change (e.g., to deliver more magnetically enriched EM1 during high MS intervals; Figures 10d and 10e). Bulk M_{rs}/M_s values in MD95-2009 (median = 0.174; IQR = 0.167–0.180) suggest significant contributions from EM3 (e.g., Figure 10d) and during IS8 and IS7 increases in bulk M_{rs}/M_s are accompanied by increases in both MS and the mean size of the <10 um fraction (Figure 12). However, sediment grain size changes cannot explain the observed covariance as a coarsening of sediment texture in EM3 dominated sources results in lower bulk M_{rs}/M_s values (Figures 7 and 11). Instead, if we assume that increases in the mean grain size and bulk MS values (Figure 11) is a response to strengthened bottom currents, then higher bulk M_{rs}/M_s values in MD95–2009 can be explained by greater access to, and transport of, EM1 and EM2 type sources across the Iceland Plateau. Particle size specific analysis of the two bulk

magnetic property records would give insights into differences in phasing in H4 and early IS8, however, this dominantly source driven interpretation is supported by coeval increases in the smectite/illite ratio and the Ti/K ratio, that were interpreted by Ballini et al. (2006) to reflect greater sourcing of basaltic derived material.

Bulk M_{rs}/M_s values in cores MD95-2010 and PS2644-5 range between 0.13–0.20 and 0.19–0.23, respectively (Kissel et al., 1999), highlighting the importance of EM3-type sources to these locations throughout Marine Isotope Stage 3. Slightly higher and less variable M_{rs}/M_s values in PS2644-5 potentially points to greater contributions of the more proximal EM1 and EM2 type sources compared to MD95-2010 that is located east of the Norway Basin on the Vøring Plateau. These data are consistent with, and are driven by, a sediment sourcing regime that draws on geological heterogeneities across the basin. Indeed, to explain the variance observed in MD99-2009 that is located in the heart of the NBP requires contributions of sediment from sources located both within and outside of the region classically referred to as the NBP. By shifting our thinking from a framework that assumes magnetic grain size scales ubiquitously with sediment grain size to one that accepts sediment sourcing as a more or less equally important process, permits a more complete interpretation, and potentially proper attribution of the bulk magnetic records. These findings open up new insights into the factors that drive bulk magnetic variability across the NNA.

6. Conclusion

By repeating the same magnetic measurements made on 71 core top bulk sediments and their five constituent sediment particle sizes we decomposed the bulk magnetic property values and assessed their sensitivity to changes in sediment texture and sediment source. Across the Edisto array clay size fractions make up a significant portion of the bulk sediment, however, they contribute far less to the bulk magnetic property values than their physical abundance suggests. In contrast, higher concentrations of ferrimagnetic minerals in the silt-size fractions results in medium silt influencing bulk MS values almost twice as much than would be suggested from its abundance alone. Hysteresis properties and low temperature MS behavior of the medium silt size fraction reveals a strong spatial signature that is driven by the contribution of materials from three distinct end members across the Nordic Seas. By modeling the magnetic response to changes in sediment texture we show that downcore changes in physical grain size can help explain the bulk magnetic record but also that sediment source changes play a substantial role in defining the bulk magnetic properties across the NBP. These results force us to shift in how we think about and interpret bulk magnetic records from a paradigm that invokes a transport dominated system to one where sediment source plays an equal if not a more important role in driving the observed variability.

Acknowledgments
This research was supported by National Science Foundation (NSF) awards OCE-1636381 (Hatfield and Stoner) and EAR-0421457 (Housen). The authors would also like to thank the NSF funded (OCE-1558679) Marine and Geology Repository at Oregon State University (OSU-MGR) for access to, and careful curation of, the 70 Edisto cores, without which this study would not have been possible. R.G.H. would like to thank Cristina Garcia Lasanta at WWU for assistance in acquiring FORC data. Reviews from Toshi Yamazaki and an anonymous reviewer improved this manuscript. Data are archived in the PANGEA database (https://doi.pangaea.de/10.1594/PANGAEA.897243) and can also be found at the Oregon State University Paleo- and Environmental Magnetic Laboratory website (http://paleomag.ceoas.oregonstate.edu).

References

Ballini, M., Kissel, C., Colin, C., & Richter, T. (2006). Deep-water mass source and dynamic associated with rapid climatic variations during the last glacial stage in the North Atlantic: A multiproxy investigation of the detrital fraction of deep-sea sediments. *Geochemistry, Geophysics, Geosystems*, *7*, Q02N01. https://doi.org/10.1029/2005GC001070

Bianchi, G. G., & Mccave, I. N. (1999). Holocene periodicity in North Atlantic climate and deep-ocean flow south of Iceland. *Nature*, *397*(6719), 515–517. https://doi.org/10.1038/17362

Bjørklund, K. R., Cortese, G., Swanberg, N., & Schrader, H. J. (1998). Radiolarian faunal provinces in surface sediments of the Greenland, Iceland and Norwegian (GIN) seas. *Marine Micropaleontology*, *35*(1–2), 105–140. https://doi.org/10.1016/S0377-8398(98)00013-9

Bloemendal, J., King, J. W., Hall, F. R., & Doh, S.-J. (1992). Rock magnetism of late Neogene and Pleistocene deep-sea sediments: Relationship to sediment source, diagenetic processes, and sediment lithology. *Journal of Geophysical Research*, *97*(B4), 4361. https://doi.org/10.1029/91JB03068

Brachfeld, S. A. (2006). High-field magnetic susceptibility (χ_{HF}) as a proxy of biogenic sedimentation along the Antarctic Peninsula. *Physics of the Earth and Planetary Interiors*, *156*, 274–282. https://doi.org/10.1016/j.pepi.2005.06.019

Chang, L., Roberts, A. P., Heslop, D., Hayashida, A., Li, J., Zhao, X., et al. (2016). Widespread occurrence of silicate-hosted magnetic mineral inclusions in marine sediments and their contribution to paleomagnetic recording. *Journal of Geophysical Research: Solid Earth*, *121*, 8415–8431. https://doi.org/10.1002/2016JB013109

Channell, J. E. T., Harrison, R. J., Lascu, I., McCave, I. N., Hibbert, F. D., & Austin, W. E. N. (2016). Magnetic record of deglaciation using FORC-PCA, sortable-silt grain size, and magnetic excursion at 26 ka, from the Rockall Trough (NE Atlantic). *Geochemistry, Geophysics, Geosystems*, *17*, 1823–1841. https://doi.org/10.1002/2016GC006300

Dahlgren, K., Torbjørn, I., & Vorren, T. O. (2003). Sedimentary environment and glacial history during the last 40 ka of the Vøring continental margin, mid-Norway. *Marine Geology*, *193*(1–2), 93–127. https://doi.org/10.1016/S0025-3227(02)00617-5

Day, R., Fuller, M., & Schmidt, V. A. (1977). Hysteresis properties of titanomagnetites: Grain-size and compositional dependence. *Physics of the Earth and Planetary Interiors*, *13*(4), 260–267. https://doi.org/10.1016/0031-9201(77)90108-X

Dunlop, D. J. (1986). Hysteresis properties of magnetite and their dependence on particle size: A test of pseudo-single-domain remanence models. *Journal of Geophysical Research*, *91*(B9), 9569. https://doi.org/10.1029/JB091iB09p09569

Egli, R. (2013). VARIFORC: An optimized protocol for calculating non-regular first-order reversal curve (FORC) diagrams. *Global and Planetary Change*, *110*, 302–320. https://doi.org/10.1016/j.gloplacha.2013.08.003

Elliot, M., Labeyrie, L., & Duplessy, J. C. (2002). Changes in North Atlantic deep-water formation associated with the Dansgaard-Oeschger temperature oscillations (60-10 Ka). *Quaternary Science Reviews*, *21*(10), 1153–1165. https://doi.org/10.1016/S0277-3791(01)00137-8

Grousset, F. E., Labeyrie, L., Sinko, J. A., Cremer, M., Bond, G. C., Duprat, J., et al. (1993). Patterns of ice-rafted detritus in the glacial North Atlantic (40–55°N). *Palaeoceanography*, *8*(2), 175–192. https://doi.org/10.1029/92PA02923

Halvorsen, S. (1974). Four sediment cores from the continental shelf outside Trøndelag. Retrieved from http://www.ngu.no/filearchive/NGUPublikasjoner/NGUnr_304_Bulletin_23_Haldorsen_21_31.pdf

Harrison, R. J., & Feinberg, J. M. (2008). FORCinel: An improved algorithm for calculating first-order reversal curve distributions using locally weighted regression smoothing. *Geochemistry, Geophysics, Geosystems*, *9*, Q05016. https://doi.org/10.1029/2008GC001987

Hatfield, R. G. (2014). Particle size-specific magnetic measurements as a tool for enhancing our understanding of the bulk magnetic properties of sediments. *Minerals*, *4*, 758–787. https://doi.org/10.3390/min4040758

Hatfield, R. G., & Maher, B. A. (2008). Suspended sediment characterization and tracing using a magnetic fingerprinting technique: Bassenthwaite Lake, Cumbria, UK. *Holocene*, *18*(1), 105–115. https://doi.org/10.1177/0959683607085600

Hatfield, R. G., Reyes, A. V., Stoner, J. S., Carlson, A. E., Beard, B. L., Winsor, K., & Welke, B. (2016). Interglacial responses of the southern Greenland ice sheet over the last 430,000 years determined using particle-size specific magnetic and isotopic tracers. *Earth and Planetary Science Letters*, *454*, 225–236. https://doi.org/10.1016/j.epsl.2016.09.014

Hatfield, R. G., Stoner, J. S., Carlson, A. E., Reyes, A. V., & Housen, B. A. (2013). Source as a controlling factor on the quality and interpretation of sediment magnetic records from the northern North Atlantic. *Earth and Planetary Science Letters*, *368*, 69–77. https://doi.org/10.1016/j.epsl.2013.03.001

Hatfield, R. G., Stoner, J. S., Reilly, B. T., Tepley, F. J., Wheeler, B. H., & Housen, B. A. (2017). Grain size dependent magnetic discrimination of Iceland and South Greenland terrestrial sediments in the northern North Atlantic sediment record. *Earth and Planetary Science Letters*, *474*, 474–489. https://doi.org/10.1016/j.epsl.2017.06.042

Kissel, C. (2005). Magnetic signature of rapid climatic variations in glacial North Atlantic, a review. *Comptes Rendus Geoscience*, *337*(10–11), 908–918. https://doi.org/10.1016/j.crte.2005.04.009

Kissel, C., Laj, C., Labeyrie, L., Dokken, T., Voelker, A., & Blamart, D. (1999). Rapid climate variations during marine isotope stage 3: Magnetic analysis of sediments from Nordic seas and Atlantic. *Earth and Planetary Science Letters*, *171*, 489–502. https://doi.org/10.1016/S0012-821X(99)00162-4

Kissel, C., Laj, C., Mulder, T., Wandres, C., & Cremer, M. (2009). The magnetic fraction: A tracer of deep water circulation in the North Atlantic. *Earth and Planetary Science Letters*, *288*(3–4), 444–454. https://doi.org/10.1016/j.epsl.2009.10.005

Kissel, C., Laj, C., Piotrowski, A. M., Goldstein, S. L., & Hemming, S. R. (2008). Millennial-scale propagation of Atlantic deep waters to the glacial Southern Ocean. *Paleoceanography*, *23*, PA2102. https://doi.org/10.1029/2008PA001624

Laj, C., Kissel, C., Mazaud, A., Michel, E., Muscheler, R., & Beer, J. (2002). Geomagnetic field intensity, North Atlantic deep water circulation and atmospheric D14C during the last 50 Kyr. *Earth and Planetary Science Letters*, *200*(1–2), 177–190. https://doi.org/10.1016/S0012-821X(02)00618-0

Lascu, I., Harrison, R. J., Li, Y., Muraszko, J. R., Channell, J. E. T., Piotrowski, A. M., & Hodell, D. A. (2015). Magnetic unmixing of first-order reversal curve diagrams using principal component analysis. *Geochemistry, Geophysics, Geosystems*, *16*, 2900–2915. https://doi.org/10.1002/2015GC005909

Lisiecki, L. E., & Raymo, M. E. (2005). A Pliocene-Pleistocene stack of 57 globally distributed benthic δ 18O records. *Paleoceanography*, *20*, PA1003. https://doi.org/10.1029/2004PA001071

Ludwig, P., Egli, R., Bishop, S., Chernenko, V., Frederichs, T., Rugel, G., et al. (2013). Characterization of primary and secondary magnetite in marine sediment by combining chemical and magnetic unmixing techniques. *Global and Planetary Change*, *110*, 321–339. https://doi.org/10.1016/j.gloplacha.2013.08.018

Maher, B. A. (1988). Magnetic properties of some synthetic sub-micron magnetites. *Geophysical Journal*, *94*(1), 83–96. https://doi.org/10.1111/j.1365-246X.1988.tb03429.x

Moros, M., Endler, R., Lackschewitz, K. S., Wallrabe-Adams, H. J., Mienert, J., & Lemke, W. (1997). Physical properties of Reykjanes ridge sediments and their linkage to high-resolution Greenland ice sheet project 2 ice Core data. *Paleoceanography*, *12*(5), 687–695. https://doi.org/10.1029/97PA02030

Moskowitz, B. M., Jackson, M., & Kissel, C. (1998). Low-temperature magnetic behavior of titanomagnetites. *Earth and Planetary Science Letters*, *157*(3–4), 141–149. https://doi.org/10.1016/S0012-821X(98)00033-8

Néel, L. (1955). Some theoretical aspects of rock-magnetism. *Advances in Physics*, *4*(14), 191–243. https://doi.org/10.1080/00018735500101204

Newton, A. M. W., & Huuse, M. (2017). Late Cenozoic environmental changes along the Norwegian margin. *Marine Geology*, *393*, 216–244. https://doi.org/10.1016/j.margeo.2017.05.004

Özdemir, Ö., Dunlop, D. J., & Moskowitz, B. M. (1993). The effect of oxidation on the Verwey transition in magnetite. *Geophysical Research Letters*, *20*(16), 1671–1674. https://doi.org/10.1029/93GL01483

Pirrung, M., Fütterer, D., Grobe, H., Matthiessen, J., & Niessen, F. (2002). Magnetic susceptibility and ice-rafted debris in surface sediments of the Nordic seas: Implications for isotope stage 3 oscillations. *Geo-Marine Letters*, *22*(1), 1–11. https://doi.org/10.1007/s00367-002-0090-1

Rasmussen, T. L., Thomsen, E., van Weering, T. C. E., & Labeyrie, L. (1996). Rapid changes in surface and deep water conditions at the Faeroe Margin during the last 58,000 years. *Paleoceanography*, *11*(6), 757–771. https://doi.org/10.1029/96PA02618

Rasmussen, T. L., Van Weering, T. C. E., & Labeyrie, L. (1997). Climatic instability, ice sheets and ocean dynamics at high northern latitudes during the last glacial period (58–10 KA BP). *Quaternary Science Reviews*, *16*(1), 71–80. https://doi.org/10.1016/S0277-3791(96)00045-5

Roberts, A. P., Pike, C. R., & Verosub, K. L. (2000). First-order reversal curve diagrams: A new tool for characterizing the magnetic properties of natural samples. *Journal of Geophysical Research*, *105*, 28,461–28,475. https://doi.org/10.1029/2000JB900326

Roberts, A. P., Tauxe, L., Heslop, D., Zhao, X., & Jiang, Z. (2018). A critical appraisal of the 'Day' diagram. *Journal of Geophysical Research: Solid Earth*, *123*, 2618–2644. https://doi.org/10.1002/2017JB015247

Robinson, S. G. (1986). The Late Pleistocene palaeoclimatic record of North Atlantic deep-sea sediments revealed by mineral-magnetic measurements. *Physics of the Earth and Planetary Interiors*, *42*(1–2), 22–47: https://doi.org/10.1016/S0031-9201(86)80006-1

Robinson, S. G., Maslin, M. A., & McCave, I. N. (1995). Magnetic-susceptibility variations in the Upper Pleistocene deep-sea sediments of the NE Atlantic: Implication for ice rafting and paleocirculation at the last glacial maximum. *Palaeoceanography*, *10*(2), 221–250. https://doi.org/10.1029/94PA02683

Snowball, I., & Moros, M. (2003). Saw-tooth pattern of North Atlantic current speed during Dansgaard-Oeschger cycles revealed by the magnetic grain size of Reykjanes ridge sediments at 59°N. *Paleoceanography*, *18*(2), 1026. https://doi.org/10.1029/2001PA000732

Stoner, J. S., & Andrews, J. T. (1999). The North Atlantic as a quaternary magnetic archive. In B. A. Maher & R. Thompson (Eds.), *Quaternary climates, environments and magnetism* (pp. 49–80). Cambridge: Cambridge University Press. https://doi.org/10.1017/CBO9780511535635.003

Stoner, J. S., Channell, J. E. T., & Hillaire-Marcel, C. (1995). Magnetic properties of deep-sea sediments off Southwest Greenland: Evidence for major differences between the last two deglaciations. *Geology*, *23*(3), 241–244. https://doi.org/10.1130/0091-7613(1995)023<0241:MPODSS>2.3.CO;2

Stoner, J. S., Channell, J. E. T., & Hillaire-Marcel, C. (1996). The magnetic signature of rapidly deposited detrital layers from the deep Labrador Sea: Relationship to North Atlantic Heinrich layers. *Paleoceanography*, *11*(3), 309–325. https://doi.org/10.1029/96PA00583

Stoner, J. S., Channell, J. E. T., Hillaire-Marcel, C., & Kissel, C. (2000). Geomagnetic paleointensity and environmental record from Labrador Sea Core MD95-2024: Global marine sediment and ice core chronostratigraphy for the last 110 kyr. *Earth and Planetary Science Letters*, *183*(1-2), 161–177. https://doi.org/10.1016/S0012-821X(00)00272-7

Thompson, R., & Oldfield, F. (1986). *Environmental magnetism*. London: Allen & Unwin. https://doi.org/10.1007/978-94-011-8036-8

Turon, J. L., Hillaire-Marcel, C., & Shipboard Participants. (1999). IMAGES V Mission of the Marion Dufresne, Leg 2, 30 June to 24 July 1999." http://publications.gc.ca/collections/collection_2016/rncan-nrcan/M183-2-3782-eng.pdf

Usui, Y., Shimono, T., & Yamazaki, T. (2018). Rock magnetism of quartz and feldspars chemically separated from pelagic red clay: A new approach to provenance study. *Earth, Planets and Space*, *70*, 153. https://doi.org/10.1186/s40623-018-0918-1

Watkins, S. J., & Maher, B. A. (2003). Magnetic characterization of present-day deep-sea sediments and sources in the North Atlantic. *Earth and Planetary Science Letters*, *214*(3–4), 379–394. https://doi.org/10.1016/S0012-821X(03)00422-9

Worm, S. E. (2016). "Tracking the sources of marine sediments on the Norwegian Sea continental shelf by using geochemical properties of detrital quartz." Masters Thesis: The Arctic University of Norway. Retrieved from https://core.ac.uk/download/pdf/43620549.pdf